

# Referencet seismic crustal model of the Dinarides

Katarina Zailac<sup>1</sup>, Bojan Matoš<sup>2</sup>, Igor Vlahović<sup>2</sup>, Josip Stipčević<sup>3</sup>

- 5 1 University of Zagreb University Computing Centre - SRCE, Zagreb, 10000, Croatia  
2 Faculty of Mining, Geology and Petroleum Engineering, University of Zagreb, Zagreb, 10000, Croatia  
3 Department of Geophysics, Faculty of Science, University of Zagreb, Zagreb, 10000, Croatia

Correspondence: Josip Stipčević (jstipcevic.geof@pmf.hr)

10

## Abstract

Continental collision zones are structurally one of the most heterogeneous areas intermixing ~~various different~~ ~~various~~ units within relatively small space. The good example of this are the Dinarides where thick carbonates ~~complex~~ cover ~~overlains~~ older crystalline basement units and remnants of subducted oceanic crust. This is further complicated by the highly variable crustal thickness ranging from 20 to almost 50 km. In terms of spatial extension, this area is relatively small, but covers tectonically very differentiated domains making ~~any seismic or geological~~ the analysis complex, with significant challenges in areas ~~that with~~ ~~lack of information on crustal structure~~ ~~less data coverage~~.

15 Presently there is no ~~comprehensive~~ ~~complete~~ 3-D crustal model of the Dinarides (and the surrounding -areas). Using the compilations of previous studies, we have created vertically and laterally varying crustal models defined on a regular grid for the wider area of the Dinarides, also covering parts of Adriatic Sea and SW part of the Pannonian Basin. We have used kriging interpolation to obtain the model parameters. In addition to the seismic velocities (P- and S-) and density, three interfaces in our model were defined – Neogene deposits bottom, Carbonate ~~rock~~ ~~complex~~ bottom and Moho discontinuity. Neogene deposits and the Paleozoic to Eocene ~~c~~ ~~Carbonate~~ ~~complex~~ rocks are not present in all areas of the model whereas Moho discontinuity depth is defined for the entire model. To validate the ~~The~~ newly derived model, we have calculated travel times for a regional earthquake recorded on a number of seismic stations in the Dinarides area. The calculated travel times ~~have~~ been compared with the travel times in the simple 1D model used for routine earthquake location in Croatia, and it proved to be a significant improvement.

25 The model derived in this work represents the first step towards improving our knowledge of the crustal structure in the complex area of the Dinarides. We hope that the newly assembled model will be useful for all the forthcoming studies (e.g. as a starting model for seismic tomography, as a model for earthquake simulations) which require knowledge of the crustal structure.

35

## Introduction

40 First seismic investigation done in the wider Dinarides region can be traced to Mohorovičić's famous discovery of the boundary between Earth's crust and mantle (Mohorovičić, 1910). The earliest deep seismic sounding experiments investigating the crustal structure beneath the Dinarides were conducted in the 1960s (Dragašević and Andrić, 1975; Aljinović, 1983; Aljinović et al., 1987). The most important results from those early investigations were about  
45 thickness of the upper crust ~~carbonate cover~~ (Aljinović, 1983). In more recent times, there was another set of active seismic experiments, the ALP 2002 (Brückl et al., 2007) focused on the investigation of the Eastern Alps but also covered the northernmost part of the Dinarides and the Pannonian basin. As part of the same international experiment, Šumanovac et al. (2009) modeled velocities in the crust and uppermost mantle from the measurements taken  
50 along the Alp07 profile located at the crossing between NW Dinarides and SW margin of the Pannonian basin. The results from the Alp07 profile were later extended by several studies including gravimetric modeling, P-wave receiver function analysis and local earthquake tomography (Šumanovac, 2010; Šumanovac et al., 2016; Orešković et al., 2011; Kapuralić et al., 2019), covering only the NW part of the Dinarides and SW part of the Pannonian basin.  
55 These studies reported a two-layer crust ~~in the area of~~ the Dinarides, and ~~virtually~~ one-layer crust in ~~the area of~~ the Pannonian basin.

The first Moho map of the Dinarides was compiled by Skoko et al. (1987) utilizing gravimetric data from that area. Similarly, Šumanovac (2010) used results from active seismics (Alp07) to calibrate gravimetric data in the Dinarides and get a more accurate map  
60 of Moho depths in the region. Stipčević et al. (2011) were first to use direct seismic measurements in the central and southern Dinarides extending the analysis of Moho depths to that region. For this they employed the P-wave receiver functions (PRF) method and by modeling it found an intra-crustal reflector ~~in the area of~~ the Internal Dinarides. Stipčević et al. (2020) extended the PRF analysis by including significantly more stations, and created  
65 the map of Moho depths beneath the Dinarides. In that extended receiver function study, Stipčević et al. (2020) report significantly thicker crust ~~in the area of~~ the southern Dinarides compared to the previous studies.

In line with the crustal exploration there have also been some recent investigations of the uppermost mantle. Using the S-wave receiver functions (SRF-) Belinić et al. (2018) mapped  
70 the lithosphere-asthenosphere boundary (LAB) under the Dinarides. The most interesting feature of that LAB map is the lack of deep lithospheric root beneath the central Dinarides, which was interpreted as thinning of the lithosphere due to possible lithospheric mantle delamination. Two years later, there was a complementary study by Belinić et al. (2020), using the Rayleigh wave tomography ~~in order to~~ obtain the upper mantle S-wave velocity

75 model for the greater Dinarides area. Similarly to their first work, authors reported missing deep lithospheric root ~~under in the area of~~ the central Dinarides, with a deep high velocity anomaly visible in the south Dinarides.

80 From this short outline of the main geophysical investigations done in the wider Dinarides area it is obvious that the crustal structure of the region is fairly complex with quite a long history of geophysical exploration. Despite this, there has never been an attempt (as far as we know) to combine these results in order to create an extensive regional 3-D crustal model for the Dinarides. The area was covered by the global and continental scale models, but the authors of these studies pointed out the lack of available data in the Dinarides area (e.g., Grad et al. 2009, Molinari and Morelli 2011, Artemieva et al., 2013). Regional scale crustal models are an important factor in all seismic studies relying on waveform modeling and seismic wave travelttime inversion. This is especially exacerbated in the areas with complex crustal structure such as the Dinarides. Therefore, it is necessary to assemble a comprehensive, ready-to-use model based on all the available results.

85 ~~Furthermore, there have been recent seismic studies in the area of the Dinarides, both of the crust and uppermost mantle, which shed light on previously poorly studied parts of this region.~~ In this study we ~~will~~ focus on the crust, and include all the data regarding crustal structure available to us, into a 3-D model covering the area of the Dinarides. The aim is to create vertically, and laterally varying crustal model defined on a regular grid for the wider area of the Dinarides using the kriging interpolation. We estimate that this model will be a good starting point for both body and surface wave tomography studies and provide an excellent base model for local and regional physics-based earthquake shaking scenarios. Besides the velocity as the main parameter describing the crustal structure, we ~~have~~ also included existing data on the Moho discontinuity depth, and the approximate Carbonate rock complex (CRC) thickness in ~~the area of~~ the Dinarides. Even though our crustal model is focused on the Dinarides, part of it also covers the SW margin of the Pannonian basin and Adriatic Sea (Fig. 1).

## Tectonic and geological setting

105 The Alpine–Carpathian–Dinaridic–Albanide–Hellenic orogenic system is a part of a Circum-Mediterranean orogenic system. Encircling the Neogene Pannonian Basin System (PBS), this orogenic system is constructed of tectonostratigraphic units derived from both Adriatic microplate and European plate that were separated by Neotethyan ocean (Schmid et al., 2008, 2020, and references therein). Tectonic units were amalgamated by fold-and-thrust systems of different polarity facing either European foreland (e.g., Western and Eastern Alps, and Carpathians) or Adriatic foreland (e.g., Southern Alps, Dinarides, Albanides, Hellenides)

110 as a result of change in subduction polarity between the European plate and Adriatic  
Microplate (Schmid et al., 2008, 2020; Ustaszewski et al., 2008).

The tectonic evolution of these large orogenic systems, i.e., Dinarides *sensu lato*, started with  
the Triassic (c. 220 Ma) opening of the Neotethys oceanic embayment between the African  
and Eurasian Plates. The Neotethys Ocean continued spreading during Late Triassic and  
115 Early to Mid-Jurassic, being interrupted only by intra-oceanic subduction of Western Vardar  
oceanic domain and ophiolite obduction onto the eastern margin of the Adriatic Microplate  
(see Schmid et al., 2020 for details). According to Schmid et al. (2008) Neotethys Ocean, i.e.,  
the Eastern Vardar oceanic domain remained open through the Late Jurassic–Cretaceous  
period (see Ustaszewski et al., 2009 and references therein).

120 The final closure of the Neotethys oceanic realm coincided with Adria Microplate and  
European foreland collision during Late Cretaceous–Early Paleogene (Schmid et al., 2020  
and references therein) that initiated formation of the Dinarides (Środoń et al., 2018). During  
the Middle Eocene–Oligocene the regional NE–SW oriented compression caused NE-directed  
continental subduction and formation of complex fold-and-thrust sheets in Dinaridic region  
125 due to SW-directed thrusting of Adria derived units, whereas in the internal Dinaridic  
domains, E–W oriented compression caused formation of the W-directed thrusting of the  
Tisza Mega-Unit over the Internal parts of the Dinarides (e.g., Handy et al., 2019; Schmid et  
al., 2020; Balling et al., 2021 and references therein). Continuous convergence of the Adria  
indenter towards the European foreland in the Late Oligocene–Early Miocene further  
130 contributed to nappe stacking and thrusting in the Alps and Dinarides, but it also  
accommodated c. 400 km E-directed orogen-parallel lateral extrusion of the ALCAPA block  
(including the Eastern Alps, West Carpathians and Transdanubian ranges north of the Lake  
Balaton) and active “back-arc-type” extension in the PBS (Royden and Horváth, 1988;  
Ratschbacher et al., 1991a, b; Frisch et al., 1998; Fodor et al., 1998; Tari et al., 1999; Csontos  
135 and Vörös, 2004; Horváth et al. 2006; Cloetingh et al., 2006; Schmid et al., 2008).

With an area of 80–200 km wide and nearly 700 km long, the Dinarides are a fold-and-thrust  
orogenic belt constructed from thrust sheets divided into ~~internal~~~~external~~ and  
~~external~~~~internal~~ tectonic domains (see Fig. 1). ~~Both tectonic domains are comprised by~~  
~~lithological units formed on either proximal or distal portions of Adria Microplate that~~  
~~represents passive margin of the Adria Microplate or its Mesozoic carbonate platform (Adria~~  
~~Carbonate Platform, i.e., AdCP), respectively. As a result, the lithological succession in the~~  
140 ~~Internal~~ Dinarides is characterized by ~~Internal Dinaridic~~ units that comprise ~~passive margin~~  
ophiolitic succession and pelagic derived sedimentary rocks, while External  
~~Dinarides~~~~Dinaridic~~ units are dominated ~~mainly~~ by ~~mainly Mesozoic~~ shallow marine  
145 carbonate ~~platform deposit~~~~complex~~ that in places reach ~~c.~~ 8000 m ~~of thickness~~ (Vlahović et  
al., 2005). Due to paleogeographic differences and tectonic complexity, Dinaridic lithological



succession is spatially highly varied in its thickness and exposure (Vlahović et al., 2005, Schmid et al., 2020; Balling et al., 2021).

150 The oldest rocks cropping out in the External Dinarides are Carboniferous to Middle Triassic  
siliciclastic-carbonate deposits accumulated along the ~~Gondwanian~~Gondwana passive  
continental margin, which due to regional extensional tectonics marked by Middle Triassic  
volcanism differentiated the area forming isolated shallow marine carbonate platforms  
155 (Vlahović et al., 2005). Through the Middle Triassic-Cretaceous timespan carbonate  
platforms in the region were surrounded by deeper marine areas, and characterized by  
mostly continuous shallow-marine carbonate deposition, though the last extensional phase  
in Toarcian ~~resulted~~resulting in disintegration in several smaller platforms, including  
Adriatic Carbonate Platform, Apenninic Carbonate Platform and Apulian Carbonate Platform  
(Vlahović et al., 2005 and references therein). During the 120 My of the AdCP's existence, i.e.,  
160 from Early Jurassic to Late Cretaceous (locally even to early Paleocene – Tešović et al., 2020),  
the thickness of deposited carbonate succession reached between 3500 and 5000 m  
(Vlahović et al., 2005 and references therein). The AdCP deposition ended due to regional  
emergence in the Late Cretaceous-Paleogene, which was linked and enhanced by tectonic  
deformations and continent collision of the Adria Microplate and European foreland yielding  
deposition of synorogenic turbiditic flysch deposits ("flysch") in newly formed foreland  
165 (flysch)-basins (Vlahović et al., 2005; Schmid et al., 2008 and references therein). The final  
uplift of the Dinarides took place from the Middle Eocene to Oligocene (Dinaric phase; see  
Schmid et al., 2008; Balling et al., 2021 with references).

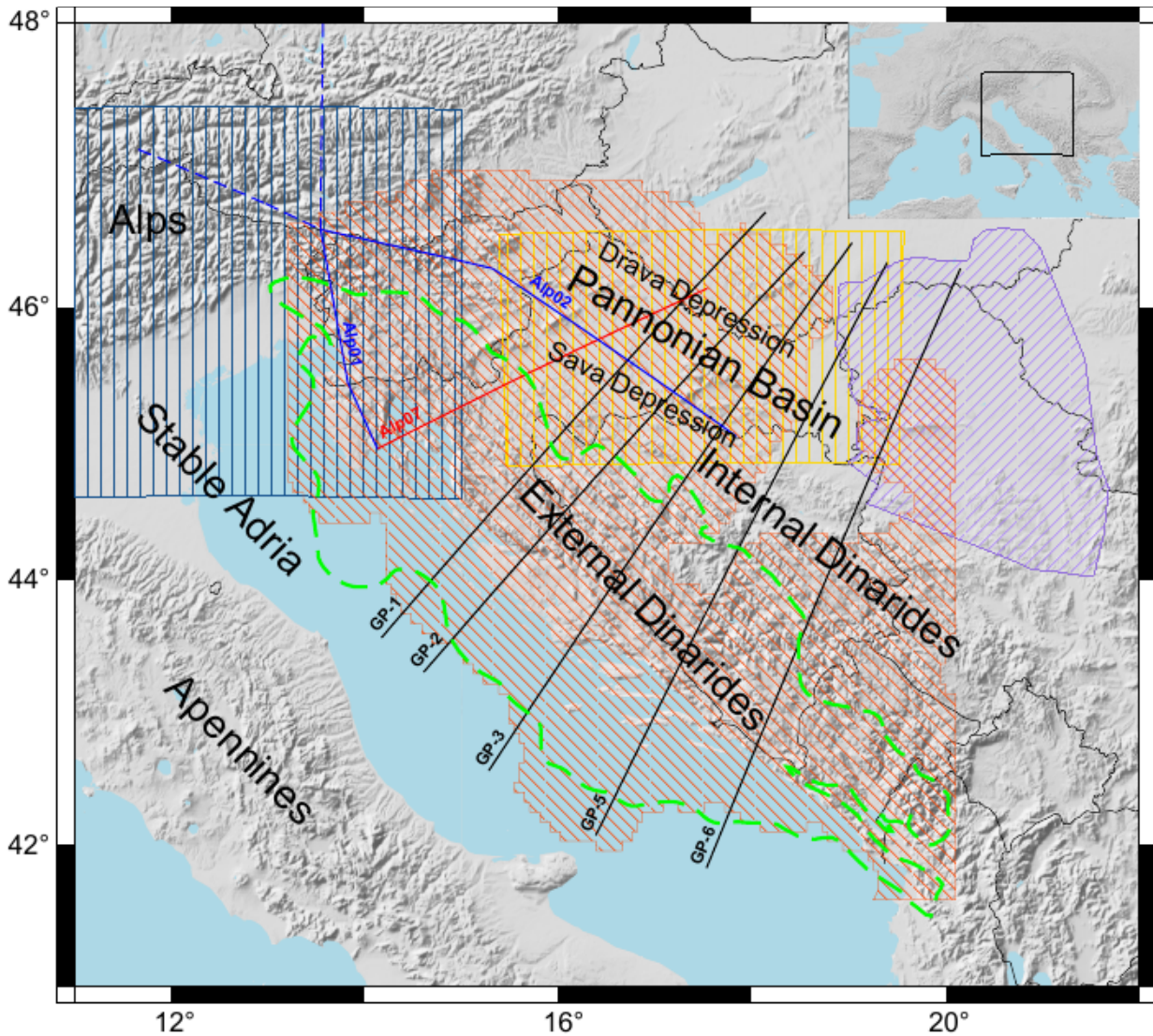
## Modeling approach ~~Data~~

170 ~~The main objective of this study is to create a referent seismic model of the crust beneath the  
Dinarides. The area covered by this investigation is somewhat wider than the Dinarides, as  
it also covers the transition zones towards the Alps and Albanides, SW part of the Pannonian  
basin and parts of the Adriatic Sea (see Fig. 1). In terms of spatial extension, this area is  
relatively small, but covers tectonically very differentiated domains making the analysis  
complex, with significant challenges in areas with less data coverage.~~

175 ~~We have decided~~Our basic approach was to create a one-layered crust with laterally and  
vertically variable parameters ~~(seismic velocities and density)~~. The reason for a choice of  
one-layered crust was a fact that not all the input data had the interpretation of intra-crustal  
interfaces, and those that had, did the interpretation in different ways. We used seismic  
velocities and density as parameters, since that is the data was readily we had available. In  
180 ~~the course of~~During data collection and integration within the new model we realized that  
the Neogene deposits in the Pannonian Basin make up a very thick and distinct layer that  
cannot be ignored, and just incorporating it into a one-layered model would be an

185 oversimplification. In the light of the Pannonian basin sedimentary complex being  
190 significantly different from the rest of the crust we included a Neogene deposits layer on top  
of a laterally and vertically varying crust. The same goes for the [Paleozoic-  
PaleogeneMesozoic CRCCarbonate complex](#) in the Adriatic-Dinarides region as there are  
numerous studies indicating distinct reflections from the bottom of the [CRCCarbonate  
complex](#) in the seismic reflection studies (Dragašević and Andrić, 1975; Aljinović, 1983;  
Aljinović et al., 1987). Given that we had no available data on any of the layer's parameters  
195 (velocity or density) in the [CRCCarbonate complex](#), we only included the [CRC  
bottomCarbonate layer](#) depth in our model. ~~TheHere,~~ velocity and density of the  
[CRCcarbonate layer](#) were ~~not interpolated separately, but were interpolated obtained~~ using  
the same [input](#) velocity (and density) data we had available for the rest of the crust. This  
choice seems reasonable, since each of the profiles used ~~actually~~ crosses the part of the  
investigated area covered with carbonates, and samples its features, even though none of the  
studies used explicitly interpreted carbonates as a separate layer.

200 To compile the data for the new crustal model, we used all available and published results.  
Some of them were not available in a digital form (mostly the studies published before 2010);  
and had to be digitized manually. The datasets used are very diverse: including two 3-D  
crustal models (one consisting of two-layered crust with interface depths while other had  
single-layered crust), several 2D interface maps (Moho depths and Neogene deposits maps),  
three seismic refraction/wide angle reflection profiles (which were the basic source for  
velocity data) and five gravimetric profiles. Coverage of the datasets used to compile the 3-  
205 D crustal model of the Dinarides is shown in **Fig. 1.** and details are listed in **Table 1.** [The  
exact locations of data points used are shown in Appendix B.](#)



210

215

**Figure 1.** Compilation of data used in this study. Blue lines mark [the positions of](#) Alp01 and Alp02 profiles (Brückl et al., 2007) – only the full line parts are used in the study; the red line is [the position](#) the Alp07 profile (Šumanovac et al., 2009); black lines are [the positions of](#) gravimetric profiles GP-1 to GP-6 (Šumanovac, 2010). Orange shaded area shows Moho depth data coverage from the receiver function study of Stipčević et al. (2020), blue vertically shaded area is the NAC model (Magrin and Rossi, 2020). The yellow shaded area shows the extent of Saftić et al. (2003) data on the Pannonian basin Neogene deposits, and the purple shaded area shows the extent of data on the Pannonian basin Neogene deposits from Matenco and Radivojević (2012). Green dashed line marks the extension of the AdCP [Carbonate rock complex](#) from Tišljar et al. (2002). The sources of the data shown in this map are listed in **Table 1**.

220 **Table 1.** List of the data sources used for the Dinarides crustal model.

Profile, model, or project name	Data type	Reference	How were data processed/obtained	Parameter that data were used for
Alp01 and Alp02	Seismic refraction and wide-angle reflection	Brückl et al. (2007)	profiles manually digitized	Vp, Moho
Alp07	Seismic refraction and wide-angle reflection	Šumanovac et al. (2009)	profile manually digitized	Vp, Moho
GP-1, GP-2, GP-3, GP-5, GP-6	2D gravity modeling	Šumanovac (2010)	profiles manually digitized	Vp, density, Moho
	Receiver functions	Stipčević et al. (2020)	available in digital form	Moho
The Northern Adria Crust (NAC) model	Multiple data sets	Magrin and Rossi (2020)	available in digital form	Vp, density, Moho
	Isopach map	Saftić et al. (2003)	digitized manually	Neogene deposits bottom depth
	Multiple data sets	Matenco and Radivojević (2012)	digitized manually	Neogene deposits bottom depth
	Carbonate rock complex distribution	Tišljar et al. (2002)	digitized manually	<a href="#">CRC</a> carbonate bottom depth
	<a href="#">Geological map</a>	<a href="#">Basic Geological Map (1:100,000) of</a>	<a href="#">digitized manually</a>	<a href="#">CRC</a> bottom depth

		<a href="#">former Yugoslavia (Osnovna Geološka Karta SFRJ)</a>		
	<a href="#">Geological map</a>	<a href="#">1:200,000 Geological Map of Albania (Geological Map of Albania, 2002)</a>	<a href="#">digitized manually</a>	<a href="#">CRC bottom depth</a>
	<a href="#">Constructed and balanced geological cross-sections</a>	<a href="#">Balling et al., (2021)</a>		<a href="#">CRC bottom depth</a>
EPcrust		Molinari and Morelli (2011)	available in digital form	Vp, Moho
SRTM15+V2.0	Global elevation grid	Tozer et al. (2019)	available in digital form	Topography

225 [We decided to use kriging for interpolation. Since kriging requires Cartesian coordinates, we transformed the data to ETRS89-extended/LAEA Europe<sup>1</sup> Cartesian coordinate system, which is defined on the entire investigated area. The transformations were done using the pyproj package \(Snow et al. 2021\). Kriging interpolation was done using the gstat package \(Pebesma, 2004\). Interface data were interpolated on a regular 5 km × 5 km grid, and the velocity and density were interpolated on a slightly more complicated grid: the horizontal grid is the same as for the interfaces \(5 km × 5 km\), but the vertical spacing changes depending on depth \(in the first 10 km of depth, the spacing is 0.5 km; between depths of 10](#)  
230 [km and 20 km, vertical spacing is 1 km, and at greater depths, vertical spacing is 2.5 km\). This scheme was used to account for better sampling and more heterogeneous upper crust.](#)

[Initially, we specified a relatively large area between 10° and 22° east longitude and 39° and 48° north latitude as the starting region of investigation. We performed interpolation in the entire initial region for each interface separately.](#)

---

<sup>1</sup> <https://epsg.io/3035>



235 Kriging does not allow multiple values at a single point in space (i.e. there is no overlapping).  
Therefore, we needed to handle the overlapping of data from various sources, before starting  
the interpolation. We tried to reduce subjectivity as much as possible, and therefore included  
known and estimated variances into the data processing. In case of the data overlapping, we  
240 calculated the value which were interpolated (depth for interfaces or velocity/density for  
layer parameters) at the given point as a weighted mean of multiple values from different  
sources, with inverse of variances used as weights:

$$\hat{d}_m = \frac{\sum_i \frac{1}{\sigma_i^2} d_{m,i}}{\sum_i \frac{1}{\sigma_i^2}},$$

where  $d_{m,i}$  is the value at point  $i$ , and  $\sigma_i^2$  is variance at point  $i$ .

245 We also included error estimates in the final model. To calculate the total error of the model,  
we followed the procedure applied by Magrin and Rossi (2020) for the derivation of the NAC  
model. With the assumption of Gaussian distribution of errors, the total variance of the  
model is the sum of two terms: the variance of the input data, and the variance from the  
interpolation itself. The interpolation variance term was provided by the gstat package along  
with the interpolated data. In order to calculate the variance at each grid point, we  
250 interpolated the input data variances on the same grid as the data itself.

There are ~~four~~three interfaces defined in the presented model – ~~CRC~~Carbonate complex  
bottom, Neogene deposits bottom, ~~and~~—Mohorovičić discontinuity (Moho), ~~and~~  
~~topography/bathymetry~~. It should be noted that not all ~~of~~ the interfaces are defined at all  
255 locations in the model (except for Moho ~~and topography/bathymetry~~). The parameters of  
the model (seismic velocities and density) are defined on a regular grid, and were calculated  
differently for the Neogene deposits layer and the rest of the crust. ~~Due to the fact that there~~  
~~was no velocity nor density information readily available for the CRC~~Carbonate layer, ~~its~~  
~~parameters were not assessed separately, as was the case for the Neogene deposits layer,~~  
~~but were calculated the same way as in the rest of the crust. The CRC~~Carbonate bottom  
260 ~~interface was kept in the model for the sake of completeness.~~

In order to define the interfaces, we needed the data on their depths. The information about  
the Moho was compiled from ~~a large number of many~~ available studies. The main source of  
Moho data was the receiver function (RF) study of Stipčević et al. (2020). These data are  
digitally available as the crustal thickness map on a regular 8.3 km × 8.3 km grid (location  
265 shown in **Fig. 1** as an orange shaded area), and it includes error estimates on the same grid.  
We also included Moho data from seismic refraction and ~~wide-wide~~-angle reflection profiles  
(Brückl et al., 2007; Šumanovac et al., 2009; profiles' locations shown in **Fig. 1** as blue and



red lines, respectively), and from the gravimetric profiles (Šumanovac, 2010; black lines in **Fig. 1**). All profiles (both seismic and gravimetric) are available as figures in digital form but had to be digitized manually. Each profile was first georeferenced, and the interpreted Moho depths were digitized every 5 km along the profile's length. For the profile data there are no detailed error estimates but the authors report that the Moho interface was resolved to at least  $\pm 2\text{--}3$  km for refraction and ~~wide-wide-angle~~ reflection profiles. There are no such estimates for the gravimetric profiles. Since the reported errors are only general, we decided to include the error estimates as described in Grad et al. (2009). The authors had a similar problem while building the Moho model for the European continent, but had much more input data to come up with reasonable error estimates. According to them, the error estimates for Moho obtained from the seismic profiles should be about 6% of the Moho depth. That estimate nicely fits with the error estimates reported by Brückl et al. (2007) and Šumanovac et al. (2009) for refraction and ~~wide-wide-angle~~ reflection profiles used in this study. As for error estimates in gravimetric profiles, Grad et al. (2009) reported somewhat higher errors, of about 20% of estimated depths. Since there was no information on errors for gravimetric profiles, we used estimates from Grad et al. (2009). For the NW part of our model, the Moho data from the high-quality and digitally available Northern Adria Crust (NAC) model (Magrin and Rossi, 2020) was also included. NAC interfaces are defined on a regular  $\sim 5 \text{ km} \times 5 \text{ km}$  grid with error estimations on the same grid (location shown in **Fig. 1** as blue shaded area).

The data for the Neogene deposits base depth came from several geological studies. Largest volumes~~The most important region~~ of the study area covered with unconsolidated~~loose~~ Neogene deposits are situated in~~is~~ the SW part of the Pannonian Basin. As the basis for the definition of the Neogene sedimentary cover thickness in this region we used data from Saftić et al. (2003), which covers the southernmost part of the Pannonian Basin (yellow shaded area in **Fig. 1**). While preparing the data, we encountered the problem that missing deposits depth information for the eastern part of our study area is causing artifacts on the border of our model after the interpolation. To mitigate this, we included data from the study by Matenco and Radivojević (2012) (purple shaded area in **Fig. 1**). Data from both studies were obtained from georeferenced isolines of the Neogene deposits depths – the isolines were digitized every 5 km, which gives the impression of random spatial sampling. ~~We did not use interpolation in this step, in order not to introduce an additional interpolation error.~~ For the error estimation we again turned to the study of Grad et al. (2009), where they estimated that the error for Moho should be about 15% for manually digitized maps. Since there was no error estimate beforehand, we decided to use the same percentage for Neogene deposits depth estimate. For the NW part of the study area, we included deposits bottom information from the NAC model. The area of the Dinarides does not contain a Neogene soft deposits cover, at least not of significant thickness, ~~since~~Tsince the basement is overlain by a thick layer of Paleozoic-Paleogene~~Mesozoic~~ CRC~~Carbonate rock complex~~. Therefore, for the area of the

Dinarides, we used the ~~CRC Carbonate complex~~ distribution described in studies of Tišljarić et al. (2002) and Vlahović et al. (2005) and marked it as a zero-Neogene deposits-thickness area, although there are locally some very restricted Neogene deposits formed within few intramontane basins. Here, the ~~CRC carbonate distribution~~ border was georeferenced and digitized manually (green dashed line in **Fig. 1**).

The interface with the least data at our disposal was the Carbonate rock complex (CRC) bottom depth. The ~~CRC Carbonate complex~~ bottom depth was estimated combining geological and structural data published in available Basic Geological Map (1:100,000) of former Yugoslavia (Osnovna Geološka Karta SFRJ), Basic Geological Maps at the 1:100,000 scale with accompanying Explanatory Notes that cover entire Dinaridic area, Geological Map of Albania at the 1:200,000 scale (Geological Map of Albania, 2002) as well as geological-structural data published in studies of Tišljarić et al. (2002), Vlahović et al., (2005) and Balling et al., (2021) (see Table A1). Based on the collected data, we determined the spatial extent of the Paleozoic-Mesozoic-Paleogene ~~CRC Carbonate complex~~. ~~Since the CRC Carbonate complex represent a very distinctive layer in the Dinarides, we additionally estimated its thickness.~~ ~~Accordingly,~~ assessment of ~~CRC Carbonate complex~~ thickness was initially performed at the scale of each of more than 80 geological maps covering the study area, using thicknesses presented in geological columns on each map. Derived values of CRC thickness were further considered in respect to the deformation styles and large-scale structural relations (e.g., Balling et al., 2021). Several regional carbonate nappe systems in the External Dinarides characterized by extensive folding and thrusting could reach a combined stacking thicknesses up to 12000 m, but thicknesses are not evenly spatially distributed. Significant variability of the CRC total thickness in the Dinarides is caused by combination of (1) initial differences in thickness due to significant paleogeographic differences along the Adria Microplate passive margin, since a total thickness of the Adriatic Carbonate Platform and thick underlying and thin overlying carbonates is in the range of 4500–8000 m (Tišljarić et al., 2002; Velić et al., 2002; Vlahović et al., 2005), (2) structural position of individual nappe systems in respect to the active collision front, and (3) variable strain rates and stress orientation during the Cretaceous–Paleogene Adria–Europe collision. Nappe stacking systems in the central and southern part of the External Dinarides, where CRC is the thickest, locally incorporate up to four thrust sheets composed of different segments of the entire carbonate succession.

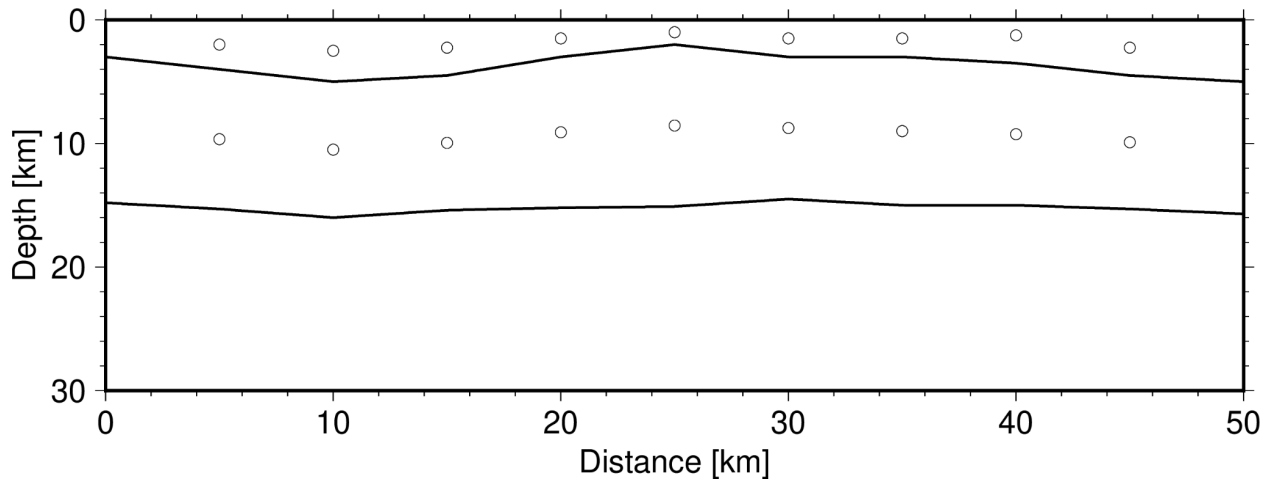
~~Derived Carbonate rock complex thickness values were further analyzed and recalculated in respect to deformation styles and large-scale structural relations (described by Balling et al., 2021). This means that the several mapped carbonate nappe systems in the Dinarides that could reach total stacking thicknesses up to 12000 m, were in most cases not evenly spatially distributed, and often were either omitted or significantly reduced. Furthermore, this implies spatial complexity of Carbonate complex stacking thicknesses in Dinarides which~~

345 were probably very unevenly enhanced from its initial thickness (c. 6000 m; see Vlahović et  
al., 2005 for details) due to inherited paleogeographic differences along the Adria Microplate  
passive margin, structural position of nappe systems in respect to active collision front, as  
350 well as variable strain rates and stress orientation during the Cretaceous–Paleogene Adria–  
Europe collision. At the same time, Dinaridic nappe stacking systems are well known in the  
central and southern part of the Dinarides where Carbonate rock succession is extremely  
thick (Fig. 3c), incorporating up to four smaller-scale thrust sheets.

As for the physical characteristics, P-wave velocities were extracted from seismic refraction  
and ~~wide-wide~~ wide-angle reflection studies (Brückl et al., 2007; Šumanovac et al., 2009), densities  
from gravimetric profiles (Šumanovac, 2010), and P- and S-wave velocities and densities  
355 from the NAC model (Magrin and Rossi, 2020). We consider P-wave velocities as the ~~best~~  
~~best~~ best-defined layer property, since there is largest number of data sources for this parameter.  
As for the S-wave velocity, there was only data from the NAC model, which is just a border  
area of our model. Therefore, we did not interpolate S-wave velocity separately, but  
estimated it from the P-wave model.

360 The NAC model is defined on a regular grid, and was easily included in our data set. The  
interpreted seismic reflection and refraction profiles (Brückl et al., 2007; Šumanovac et al.,  
2009) were digitized manually on a regular grid with the horizontal spacing of 5 km (along  
the length of each profile) and vertical spacing of 1 km. Since the gravimetric profiles are  
365 interpreted in terms of homogeneous layers (density in a layer does not change vertically  
nor horizontally), we applied a slightly different logic. We used 5 km spacing along the profile  
and instead of regularly digitizing the densities in depth, we only picked one point in each  
layer, in the middle of the layer, with assigned layer density. It seemed the most logical  
course of action, assigning the density value to the middle of the layer, as a way to represent  
the entire layer. A simplified example of gravimetric profiles digitisation is shown in **Fig. 2**.

370 We should also mention the error estimation regarding the velocity and density data. The  
NAC model (Magrin and Rossi, 2020) had reported parameter errors for each grid point and  
for interfaces, so these were simply included in our data set. Seismic refraction and ~~wide~~  
~~wide~~ wide-angle reflection profiles (Brückl et al., 2007; Šumanovac et al., 2009) had a general  
estimate of velocity error of  $\pm 0.2$  km/s and  $\pm 0.1$  km/s, respectively. In those cases, we  
375 simply assigned that globally estimated error to each digitized data point. In the case of the  
density data calculated from the gravimetric measurements there was no error estimate.  
Therefore, we had to use other results ~~in-order-to-to~~ help us quantify error for that dataset.  
Since the only other source of density data was the NAC model, and since we had no reason  
to believe that the gravimetric profiles we used (Šumanovac, 2010) are of a lower quality  
380 than those included in the NAC model, we assigned the maximum error estimate (to make a  
conservative estimate) from the NAC model to each of the points from the digitized  
gravimetric profiles.



385 **Figure 2.** Simplified example of data sampling from one the gravimetric profiles with two interpreted  
 layers. The dots represent digitized data points used to build our model. See text for details.

390 [The most accurate source of velocity data were refraction and wide angle seismic reflection profiles \(Brückl et al., 2007; Šumanovac et al., 2009\), and the NAC model \(Magrin and Rossi, 2020\) but as can be seen in Fig. 1 these studies do not cover the central and southern area of the Dinarides. Therefore, we also included velocities calculated using the values of density from gravimetric profiles \(Šumanovac, 2010\). The differences in the digitization of the gravimetric profiles have been described in the previous section. In order to calculate P-wave velocities from the available densities, we used Brocher's \(2005\) empirical equation:](#)

$$V_p = 39.128\rho - 63.064\rho^2 + 37.083\rho^3 - 9.1819\rho^4 + 0.8228\rho^5,$$

395 [where  \$V\_p\$  is P-wave velocity in km/s, and  \$\rho\$  is density in g/cm<sup>3</sup>. The equation is valid for densities between 2 and 3.5 g/cm<sup>3</sup> \(with the correlation coefficient of ~0.999\), the condition which was satisfied for all the densities in gravimetric profiles used.](#)

400 [The velocity in the Neogene deposits is poorly known so it was estimated using Brocher \(2008\) empirical relations \(eqs. 1, 3, 7, and 9 in the original article\). These relations account for increasing burden pressure, but not for variations in other factors. Therefore, it is justified to use these relations as a first-order approximation, because there are no similar relations readily available for the Pannonian Basin. We used Brocher's Plio-Quaternary relations for the shallowest parts, and relations for Paleogene-Neogene sedimentary rocks for the rest of the Neogene deposits. The values obtained ranged from around 0.7 km/s for depths close to surface, to around 5.6 km/s at greatest depth in the Neogene deposits \(which was 7.5 km below surface\).](#)

405

We used a regional EPcrust model (Molinari and Morelli, 2011) as the underlying model ~~in~~  
410 ~~order~~ to fill the gaps in the data coverage. The EPcrust model is represented by three layers:  
sedimentary cover, upper crust, and lower crust, with a horizontal resolution of  $0.5^\circ \times 0.5^\circ$ .  
Each layer is characterized by laterally varying P- and S-wave velocity and density, and all ~~of~~  
the parameters are constant for each grid point. We include EPcrust Moho, Neogene deposits  
bottom depth and velocity information only in parts with no other sources of data. This was  
415 done ~~in order to~~ remove interpolation artifacts in transition areas between the local data  
described before and the underlying EPcrust model. Therefore, we implemented a condition  
to include EPcrust data in our dataset: each grid point defined in the EPcrust model had to  
be distanced more than 100 km in each direction distant from the other data. That way, the  
data from the regional EPcrust model will not have too much influence on more relevant,  
local data.

420 For topography the SRTM15+V2.0 model (Tozer et al., 2019) was used. It is an updated  
global elevation grid at a spatial sampling of 15 arc seconds, and it also includes bathymetry.  
Since the grid of the SRTM15+V2.0 model is much more refined than the grid we used for the  
definition of our model (15 arc seconds in the topography model compared to about 3 arc  
minutes in our model), a regridding has been performed~~we included it in our model~~ by  
425 averaging all the values that fall inside our model cell.

After collecting and preparing the data, the next step was interpolation. Ordinary kriging was  
used to interpolate model interfaces and universal kriging when interpolating the layer  
properties ( $V_p$  velocity, density) as the layer properties are distinctly linearly dependent on  
depth. After interpolation, we filtered Moho discontinuity and layer properties with a 100-  
430 km wide Gaussian filter to smooth the transitions between different data sources. The  
smoothing in case of the Neogene deposits and CRC interfaces was omitted because the data  
used in derivation of those interfaces came from similar sources, and smoothing would  
conceal known structures due to their relatively small spatial dimensions (e.g. Sava and  
Drava depressions would have been concealed with smoothing).

435 We observed how the smoothing influenced the crustal velocity, particularly in the area of  
the model for which most data was provided by gravimetric profiles. Given that the  
gravimetric profiles are interpreted in terms of isotropic sections, and given that the smaller  
sections interpreted were roughly about 100 km in dimension along the profile, we chose  
this as the Gaussian width. It was also confirmed by trial and error that below this width we  
440 would observe some artifacts in the model. Model uncertainty was estimated as the sum of  
two factors: uncertainty in the input data and uncertainty from the interpolation.

## Model construction

Ordinary kriging was used to interpolate all the interface data (Neogene deposits, CRC Carbonate complex thicknesses and Moho discontinuity depths), and universal kriging to interpolate crust velocity and density data. Since kriging requires Cartesian coordinates, we transformed the data to ETRS89-extended/LAEA Europe<sup>2</sup> Cartesian coordinate system, which is defined on the entire investigated area. The transformations were done using the *pyproj* package (Snow et al. 2021). Kriging interpolation was done using the *gstat* package (Pebesma, 2004). Interface data were interpolated on a regular 5 km × 5 km grid, and the velocity and density were interpolated on a slightly more complicated grid: the horizontal grid is the same as for the interfaces (5 km × 5 km), but the vertical spacing changes depending on depth (in the first 10 km of depth, the spacing is 0.5 km; between depths of 10 km and 20 km, vertical spacing is 1 km, and at greater depths, vertical spacing is 2.5 km). This scheme was used to account for better sampling and more heterogeneous upper crust.

Initially, we specified a relatively large area between 10° and 220° east longitude and 39° and 48° north latitude as the starting region of investigation. We performed interpolation in the entire initial region for each interface separately. As mentioned in the previous section, most of the available data was related to the Moho discontinuity, and therefore the results of that interpolation are considered most accurate. Because of that, we used Moho discontinuity depth errors in combination with lower uncertainty areas of the Vp model as guidelines to mark edges of our model. The final model covers only the area between roughly 13° E and 20° E, and 42° N and 47° N.

Kriging does not allow multiple values at a single point in space (i.e. there is no overlapping). Therefore, we needed to handle the overlapping of data from various sources, before starting the interpolation. We tried to reduce subjectivity as much as possible, and therefore included known and estimated variances into the data processing. In case of the data overlapping, we calculated the value which were interpolated (depth for interfaces or velocity/density for layer parameters) at the given point as a weighted mean of multiple values from different sources, with inverse of variances used as weights:

$$\widehat{d}_m = \frac{\sum_i \frac{1}{\sigma_i^2} d_{m,i}}{\sum_i \frac{1}{\sigma_i^2}},$$

where  $d_{m,i}$  is the value at point  $i$ , and  $\sigma_i^2$  is variance at point  $i$ .

---

<sup>2</sup> <https://epsg.io/3035>



475 We also included error estimates in the final model. To calculate the total error of the model, we followed the procedure applied by Magrin and Rossi (2020) for the derivation of the NAC model. With the assumption of Gaussian distribution of errors, the total variance of the model is the sum of two terms: the variance of the input data, and the variance from the interpolation itself. The interpolation variance term was provided by the *gstat* package along with the interpolated data. In order to calculate the variance at each grid point, we interpolated the input data variances on the same grid as the data itself.

480 The right hand side of **Fig. 3** (panels b, d and f) shows the standard deviations (the positive square root of the variance) for CRC Carbonate rock thickness, Neogene deposits thickness and Moho depth. For the deposits bottom error estimation, we had the following models available: Tišljarić et al. (2002), Saftić et al. (2003), Matenco and Radivojević (2012), and Magrin and Rossi (2020) — the rest of the area was filled with regional EPerust data, and is therefore of lower accuracy.

485 The most accurate source of velocity data were refraction and wide angle seismic reflection profiles (Brückl et al., 2007; Šumanovac et al., 2009), and the NAC model (Magrin and Rossi, 2020) but as can be seen in **Fig. 1** these studies do not cover the central and southern area of the Dinarides. Therefore, we also included velocities calculated using the values of density from gravimetric profiles (Šumanovac, 2010). The differences in the digitization of the gravimetric profiles have been described in the previous section. In order to calculate P-wave velocities from the available densities, we used Brocher's (2005) empirical equation:

$$V_p = 39.128\rho - 63.064\rho^2 + 37.083\rho^3 - 9.1819\rho^4 + 0.8228\rho^5,$$

495 where  $V_p$  is P-wave velocity in km/s, and  $\rho$  is density in g/cm<sup>3</sup>. The equation is valid for densities between 2 and 3.5 g/cm<sup>3</sup> (with the correlation coefficient of ~0.999), the condition which was satisfied for all the densities in gravimetric profiles used.

500 The velocity in the Neogene deposits is poorly known so it was estimated using Brocher (2008) empirical relations (eqs. 1, 3, 7, and 9 in the original article). These relations account for increasing burden pressure, but not for variations in other factors. Therefore it is justified to use these relations as a first-order approximation, because there are no similar relations readily available for the Pannonian Basin. We used Brocher's Plio-Quaternary relations for the shallowest parts, and relations for Paleogene-Neogene sedimentary rocks for the rest of the Neogene deposits. The values obtained ranged from around 0.7 km/s for depths close to surface, to around 5.6 km/s at greatest depth in the Neogene deposits (which was 7.5 km below surface).

|

## 510 The main characteristics of the model

515 After collecting and preparing the data as described in the previous sections, the next step was interpolation. Ordinary kriging was used to interpolate model interfaces and universal kriging when interpolating the layer properties (Vp velocity, density) as the layer properties are distinctly linearly dependent on depth. After interpolation, we ~~filtered~~smoothed Moho discontinuity and layer properties with a 100 km wide Gaussian filter to smooth the transitions between different data sources, but skipped the smoothing in case of the Neogene deposits and CRC Carbonate complex layer interfaces. The smoothing in case of the Neogene deposits and CRC interfaces in those cases was omitted because the data used in derivation of those interfaces came from similar sources, and smoothing would conceal known structures due to their relatively small spatial dimensions (e.g. Sava and Drava depressions would have been concealed with smoothing). The same smoothing was applied for the Moho interface and for the crustal parameters. We observed how it influenced the crustal velocity, particularly in the area of the model for which most data was provided by gravimetric profiles. Given that the gravimetric profiles are interpreted in terms of isotropic sections, and given that the smaller sections interpreted were roughly about 100 km in dimension along the profile, we chose this as the Gaussian width. It was also confirmed by trial and error that below this width we would observe some artifacts in the model. Model uncertainty was estimated as the sum of two factors: uncertainty in the input data and uncertainty from the interpolation. The estimation of the former is described in detail in previous sections, and the latter is available from the output of kriging.

525  
530  
535 Most of the available data was related to the Moho discontinuity, and therefore the results of that interpolation are considered most accurate. Because of that, we used Moho discontinuity depth errors in combination with lower uncertainty areas of the Vp model as guidelines to mark edges of our model. The final model covers only the area between roughly 13° E and 20° E, and 42° N and 47° N.

540 Interfaces embedded within the model are shown in the left-hand side of **Fig. 3** (panels a, c and e). The shaded areas mark the region where the model is not well defined. The right hand side of Fig. 3 (panels b, d and f) shows the standard deviations (the positive square root of the variance) for CRC thickness, Neogene deposits thickness and Moho depth. For the deposits bottom error estimation, we had the following models available: Tišljarić et al. (2002), Saftić et al. (2003), Matenco and Radivojević (2012), and Magrin and Rossi (2020) – the rest of the area was filled with regional EPcrust data, and is therefore of lower accuracy. Neogene deposits and Carbonate rock complex bottom depths have not been smoothed, since they have been assembled from a small number of equivalent sources. Moho discontinuity, on the other hand, is assembled from a variety of different sources, and therefore was smoothed using a Gaussian filter with a 100 km width.

545

Since the model is mostly concentrated on the Dinarides where the topmost cover is predominantly made of ~~Paleozoic-Mesozoic~~-Eocene ~~CRCcarbonate rock complex~~, Neogene sedimentary cover is negligible for the large part of the model, but areas to the east and northeast of the Dinarides (i.e. SW Pannonian Basin) have thick Neogene deposits reaching thicknesses of more than 4 km. Most prominent features, clearly seen as two red bands in **Fig. 3a**, are the Sava and Drava depressions, with Drava depression being slightly deeper.

~~CRCCarbonates~~ bottom depth model (**Fig. 3c**) is almost a mirror image of the Neogene deposits bottom model. ~~[That was expected, since~~ in the SW Pannonian Basin, where Neogene deposits are the thickest, ~~the underlying~~ carbonate layer is thin, and vice versa – in the Dinarides, where the ~~CRCcarbonate layer~~ is the thickest, there are no prominent Neogene deposits. ~~CRCCarbonate~~ thicknesses are well over 5 km in the northern part of the ~~External~~ Dinarides and they are getting even thicker going southwards along the Dinarides chain strike (reaching cumulative thicknesses of almost 15 km in the southern part of the mountain chain). In the Adriatic Sea area, carbonates are thinning out going southwestwards, but that may also be partly caused by the relative lack of available data in that part of the model.

~~As corroborated before, Moho discontinuity depth is the best constrained feature of the model.~~ Greatest Moho depths in the investigated region are found in the ~~SESW~~ part of the Dinarides mountain chain, where it reaches depths of over 45 km (see **Fig. 3e**). To the ~~NWNE~~, along the External Dinarides mountain chain strike Moho becomes shallower, reaching depths of around 40 km. In the SW part of the Pannonian basin crustal thickness is between 20 and 30 km, becoming even shallower going further east. In the Adriatic Sea (within the part covered with our model), Moho is shallower than in the Dinarides, but deeper than in the SW Pannonian Basin, with crustal thicknesses between 30 and 35 km. At the transition from Adriatic Sea to the Dinarides mountain chain, the Moho depth change is gradual, whereas going towards the SW Pannonian basin from the Dinarides, the change is rather abrupt. ~~This can be better seen in Fig. 5, which shows three profiles laid almost perpendicularly to the strike of the Dinarides.~~

The right-hand side of **Fig. 3** (panels b, d and f) shows interface uncertainties (Neogene deposits, ~~CRCCarbonate~~ bottom and Moho depth, respectively). Given that a significant contribution to the uncertainty value is the uncertainty from the interpolation itself (which is of greater value at grid points further away from the input data points), one can distinctly see the areas with less data coverage as areas with higher uncertainty. Moho depth uncertainty (**Fig. 3f**) is low in the entire area of interest, i.e. the wider Dinarides region. For Neogene deposits bottom the area of lower data coverage is in the eastern part of the Internal Dinarides where there is less information available on sedimentary thickness (see also **Fig. 1**). On the other hand, that part of the Internal Dinarides is mostly covered by the exposed bedrock largely composed of low-grade metamorphic Paleozoic–Mesozoic formations with

585 thin cover of Mesozoic ~~CRCcarbonate rock complex~~ (e.g. Schmid et al., 2008), so Neogene  
deposits thickness values here are mostly negligible. For ~~CRCCarbonate rock layer~~ thickness,  
the area of least accuracy is in the NE part of the investigated area (junction zone between  
Dinarides-Pannonian basin-Southern Alps). Similar to the previous case, here the low  
accuracy is due to the lack of measurements on ~~CRCcarbonate~~ thickness as the region is  
590 covered by a thick layer of Neogene deposits.

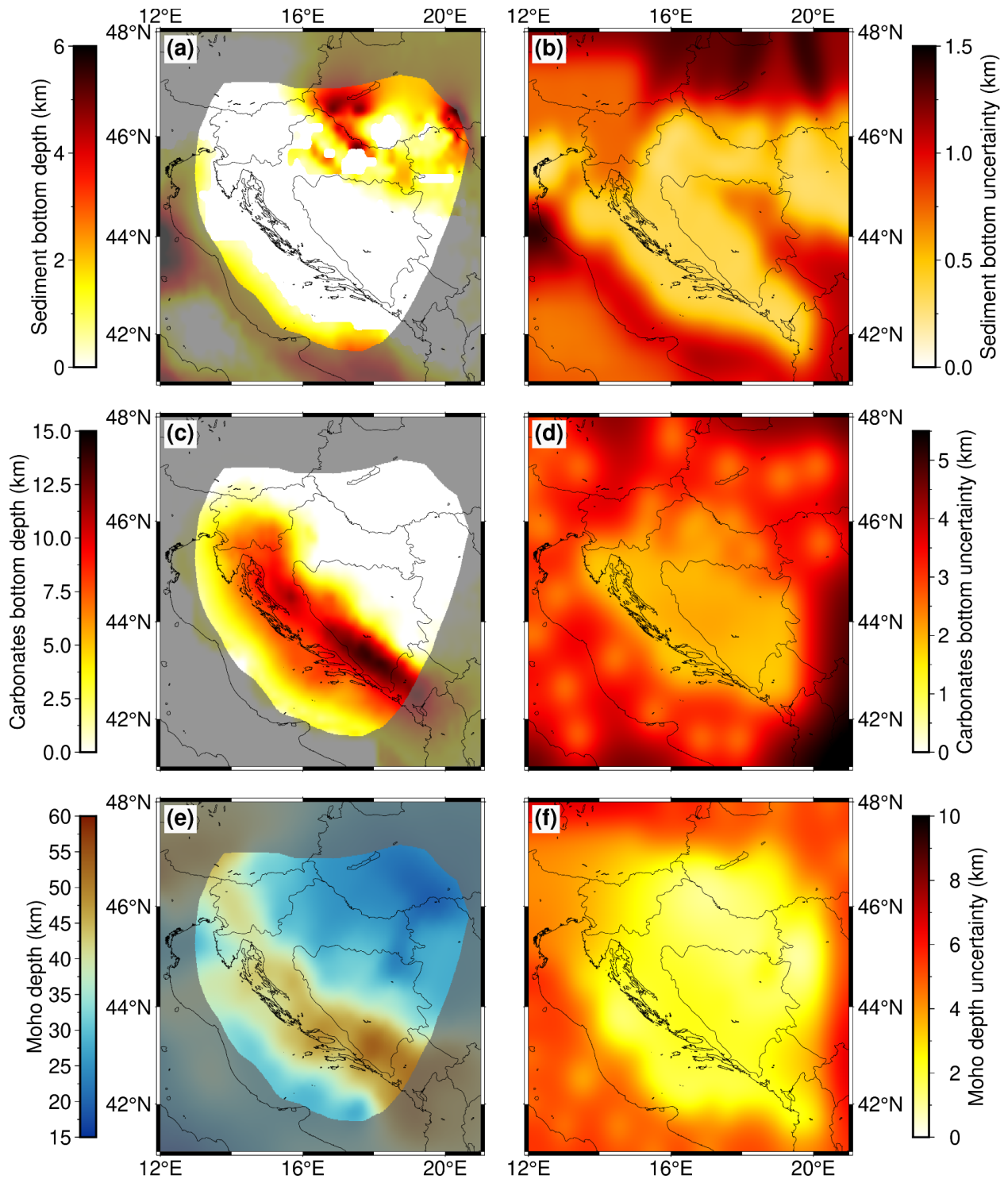
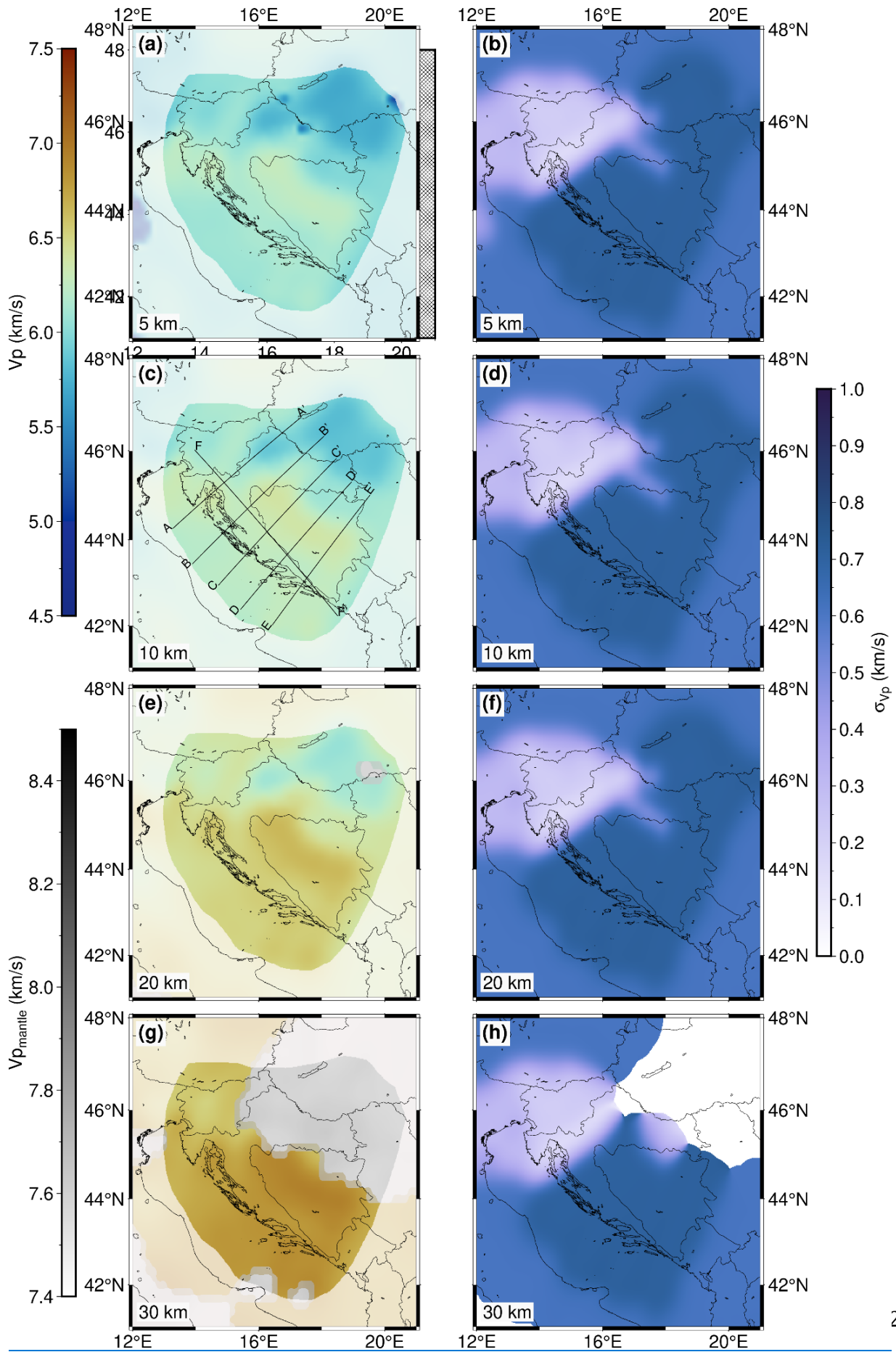


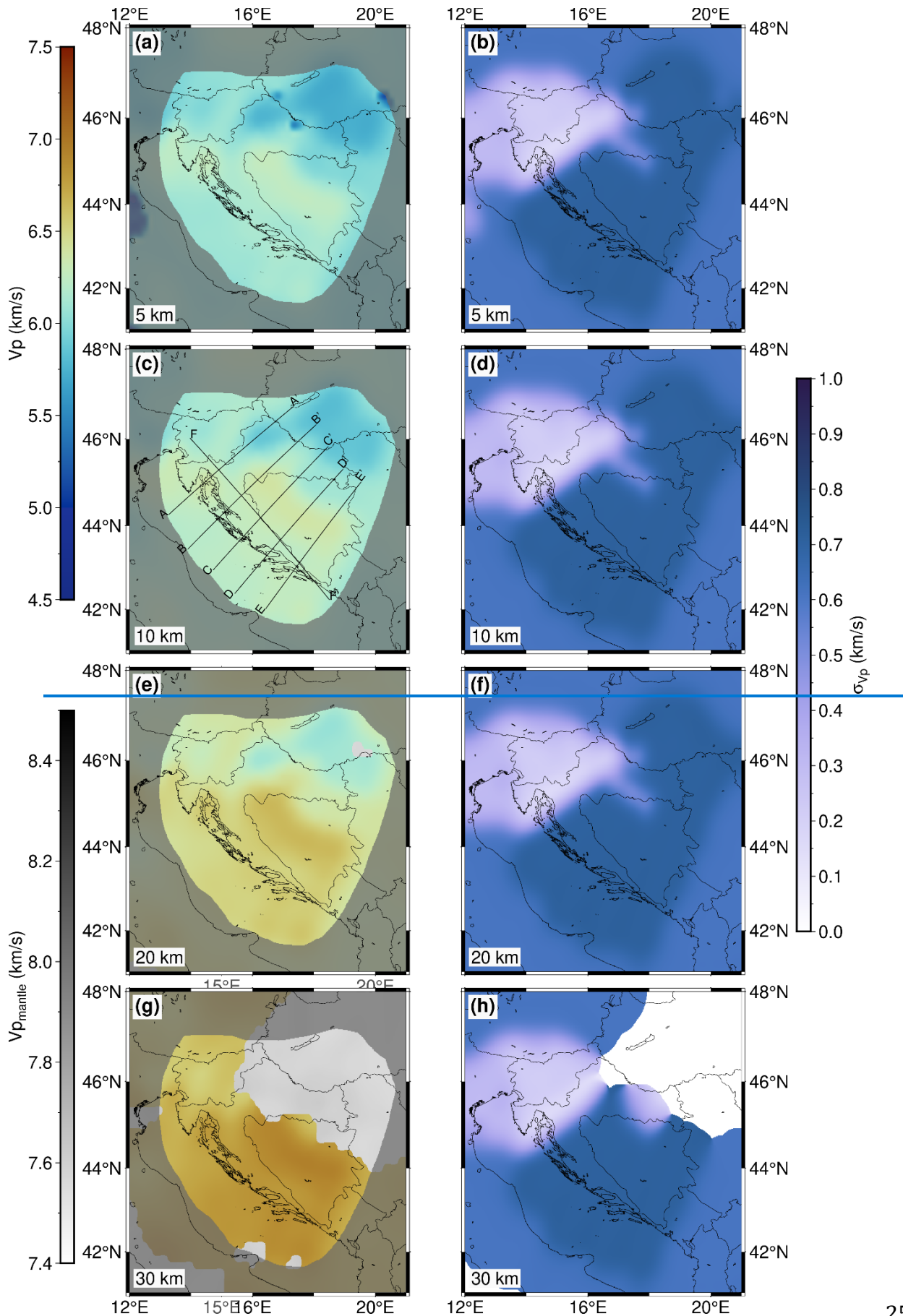
**Figure 3.** Model interface depths and corresponding uncertainties: (a) Neogene deposits bottom depth, (b) Neogene deposits bottom uncertainty, (c) [CRCCarbonate](#) bottom depth, (d) [CRCCarbonate](#) bottom uncertainty, (e) Moho discontinuity depth, and (f) Moho depth uncertainty.



The seismic velocity distribution within the model is depicted in the left-hand side of **Fig. 4** at four depths (5, 10, 20 and 30 km) showing most prominent features of the model crustal structure. At a depth of 5 km (**Fig. 4a**), the P-wave velocity in a large part of the External Dinarides is about 6 km/s. Given that we had no ~~independent~~~~separate~~ estimate for the velocity for the ~~CRC~~~~carbonate~~~~layer~~, we cannot discern it as a separate layer just looking at velocity values. ~~Outside the External Dinarides~~~~In the rest of the model~~, one can see that the velocity in the SW Pannonian Basin at depth of 5 km is slightly lower (just below 6 km/s) than than in the rest of the investigated area. At a depth of 10 km (**Fig. 4c**) the velocity values in the SW Pannonian Basin are considerably lower than in the rest of the model, with values around 6 km/s. In the area of the Internal Dinarides, velocity at 10 km depth is slightly higher than in the External Dinarides and beneath the Adriatic Sea. It is hard to discern if this reflects the actual structure, or if it is the consequence of the higher uncertainty in that part of the model (the velocity here was estimated from the density values from the gravimetric profiles, given that there were no other data sources available). Similar situation can be seen in **Fig. 4e** for a depth of 20 km. For this depth the velocities in the SW Pannonian Basin are reaching values above 6 km/s whereas values for the Dinarides are again higher (especially in the internal part) than in the rest of the investigated area, with values above 6.5 km/s. In the lower part of the crust (**Fig. 4g**) at a depth of 30 km in the central part of the Dinarides the P-velocity values are reaching 7 km/s. In the same image the mantle velocity values are shown in grayscale due to the considerable difference between crust and mantle values and the fact that the crustal thickness in SW Pannonian basin is mostly less than 25 km. The mantle velocity variations are better seen in profile sections (e.g. see **Fig. 5f**). At the 30 km depth, the velocity is much higher in the south External Dinarides and below the Adriatic Sea (at least the part covered with our model) than in the northern External Dinarides. The mantle velocity shown ~~in Figs. 4 and 5~~~~here~~ is not estimated as part of this model, but was taken from Belinić et al. (2020), by estimating it from the Vs model reported there using the standard P over S-velocity ratio for the upper mantle ( $V_p/V_s = 1.73$ ).

**Fig. 4** also shows error estimates for P-wave velocity at four depths: 5 km, 10 km, 20 km and 30 km (panels b, d, f and h, respectively). ~~It can be seen that the~~~~The~~ lowest estimates are in the area where we used the NAC model input data (Magrin and Rossi, 2020), and in areas where data from active seismic profiles were available (Brückl et al., 2007; Šumanovac et al., 2009). The disposition of the errors shown in **Fig. 4** was expected given the fact that the digital NAC model and the active seismic profiles are of highest quality and that gravimetric data has higher uncertainty. Estimated uncertainty is highest in the area where gravimetric profiles (Šumanovac, 2010) are the main source of the data used to estimate P-velocity.





635 **Figure 4.** Velocity model depth slices and corresponding uncertainties for uncertainties: P-velocity  
model depth slices for 5 km, 10 km, 20 km, and 30 km depth are shown in panels (a)(b), (c)(d), (e)(f)  
and (g)(h). (a) model at a depth of 5 km, (b) uncertainty at a depth of 5 km, (c) model at a depth of 10  
640 km, (d) uncertainty at a depth of 10 km, (e) model at a depth of 20 km, (f) uncertainty at a depth of  
20 km, (g) model at a depth of 30 km, and (h) uncertainty at a depth of 30 km. In the panel (c) the  
positions of the profiles shown in **Fig. 5** are marked. The areas of lower resolution are shaded, and  
the gray color scale corresponds to the mantle velocity (see text for details).

**Fig. 5** shows depth variations of velocity along the profiles (locations marked in **Fig. 4cb**)  
crossing the Dinarides perpendicularly with one profile (FF)' running parallel to the main  
strike of the mountain chain. The profile AA' (**Fig. 5a**) crosses the Dinarides in their northern  
645 part. The maximum Moho depth below the Dinarides on this profile (around 40 km) is the  
lowest compared to the other profiles. At a distance of ~270 km, the profile reaches the SW  
Pannonian Basin, which can be clearly seen as the thinning of the crust (between 20 and 30  
km) and by the topmost layer of Neogene deposits of lower P-velocity. Although the  
CRC Carbonate complex layer thickness is indicated with the dashed line, one cannot  
650 recognize it by looking just at the velocity values. Generally, the velocities in the part of the  
profile crossing the Dinarides are larger than in the part of the profile crossing the SW  
Pannonian Basin. The velocity gradually increases with depth, reaching values of about 6.7–  
7.0 km/s in the deepest part of the crust, with the exception of the SW Pannonian Basin,  
where the velocity just above Moho is lower, about 6.5 km/s.

655 The maximum Moho depth seen on the profile BB' (**Fig. 5b**) is somewhat greater than in the  
profile AA', a little over 40 km in the part of the External Dinarides. It is shallower in the  
Adriatic area (in the first 50 km of the profile) and in the Internal Dinarides (after about 220  
km). At the very end of the profile, where it reaches the SW Pannonian Basin, one can see the  
same feature seen in the profile AA': thinner crust and slightly lower velocity just above  
660 Moho than in the rest of the profile. The CRC Carbonate layer thickness, indicated by the  
dashed line, in the part of the profile crossing the part where Moho is the deepest, in large  
parts of the profile almost perfectly coincides with the velocity isoline value of about 6.3  
km/s. That feature can also be observed on other profiles (CC' and DD') at similar locations.

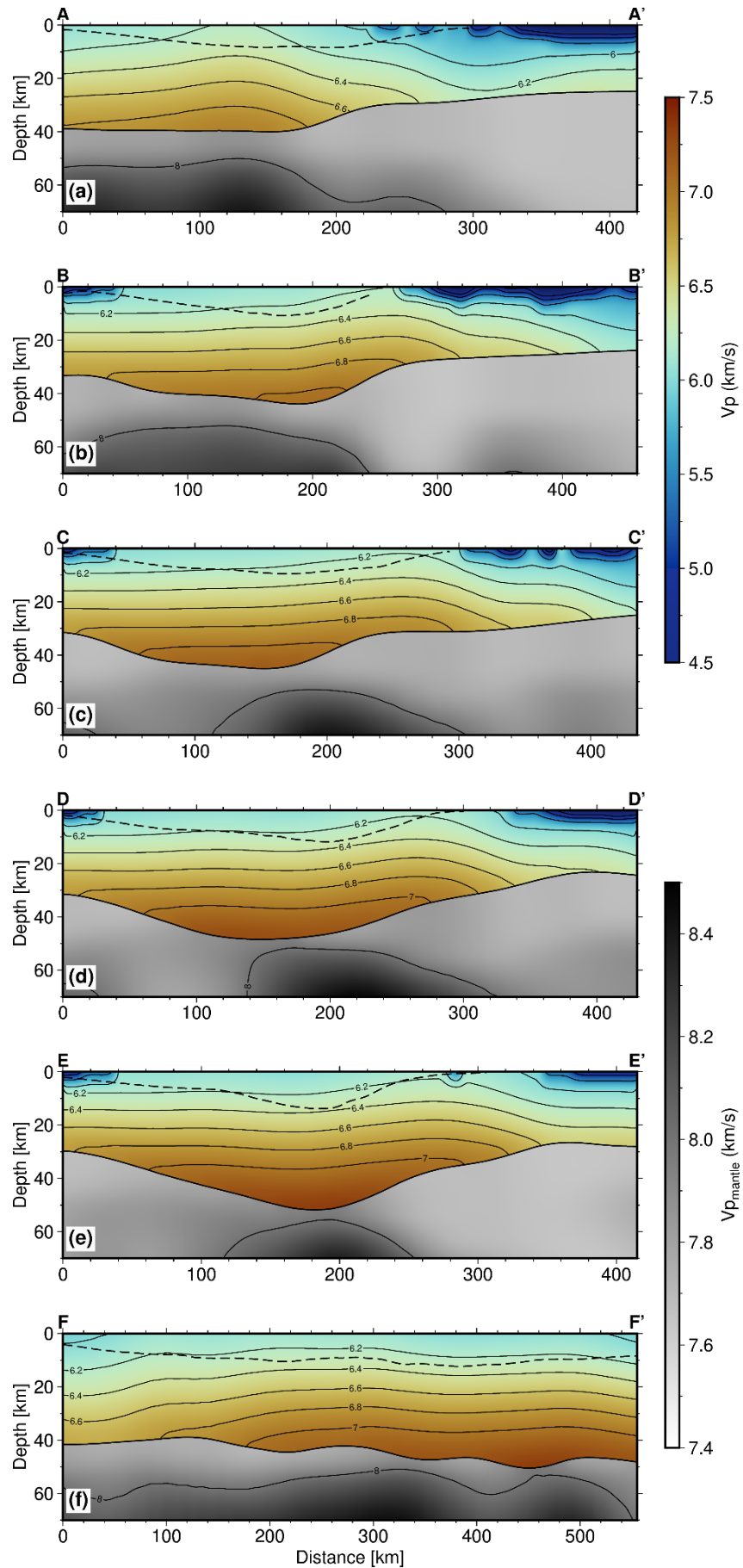
The profile CC' (**Fig. 5c**) crosses the Dinarides in their central part. Here the maximum Moho  
665 depth is almost 50 km. The profile reaches the SW Pannonian Basin only in the last 100 km,  
but it covers much of the Internal Dinarides. The CRC Carbonate layer is of uniform thickness  
along the part of the profile covering the Dinarides (after the first 100 km, which cover the  
Adriatic area). The crust is thickest beneath the External Dinarides, and is becoming thinner  
going both towards the Adriatic Sea and the Internal Dinarides. In this central part of the  
670 External Dinarides, there is also somewhat higher velocity recorded deeper in the crust, 7.0–  
7.2 km/s, just above the Moho. In the Internal Dinarides (between 250 to 300 km from the

675 start of the profile), the velocity just above the Moho is a little lower than in the external part, around 6.7–7.0 km/s. As noticed in the previous two profiles, in the SW Pannonian Basin, the velocity just above Moho is even lower than in the Internal Dinarides. Similarly, as for the profile BB', the bottom of the ~~CRC~~Carbonate layer coincides with the velocity values of about 6.2–6.3 km/s, except in the very beginning of the profile (first ~50 km). ~~In this profile (but see also profiles DD' and EE') it is worth mentioning that the higher velocity body mapped in the upper mantle (Belinić et al. 2020) coincides well with the thickest crustal section. This can be linked with the remnants of the subducted lithosphere and the ongoing underthrusting or lithospheric delamination (see e.g., discussion in Stipčević et al. 2020)~~

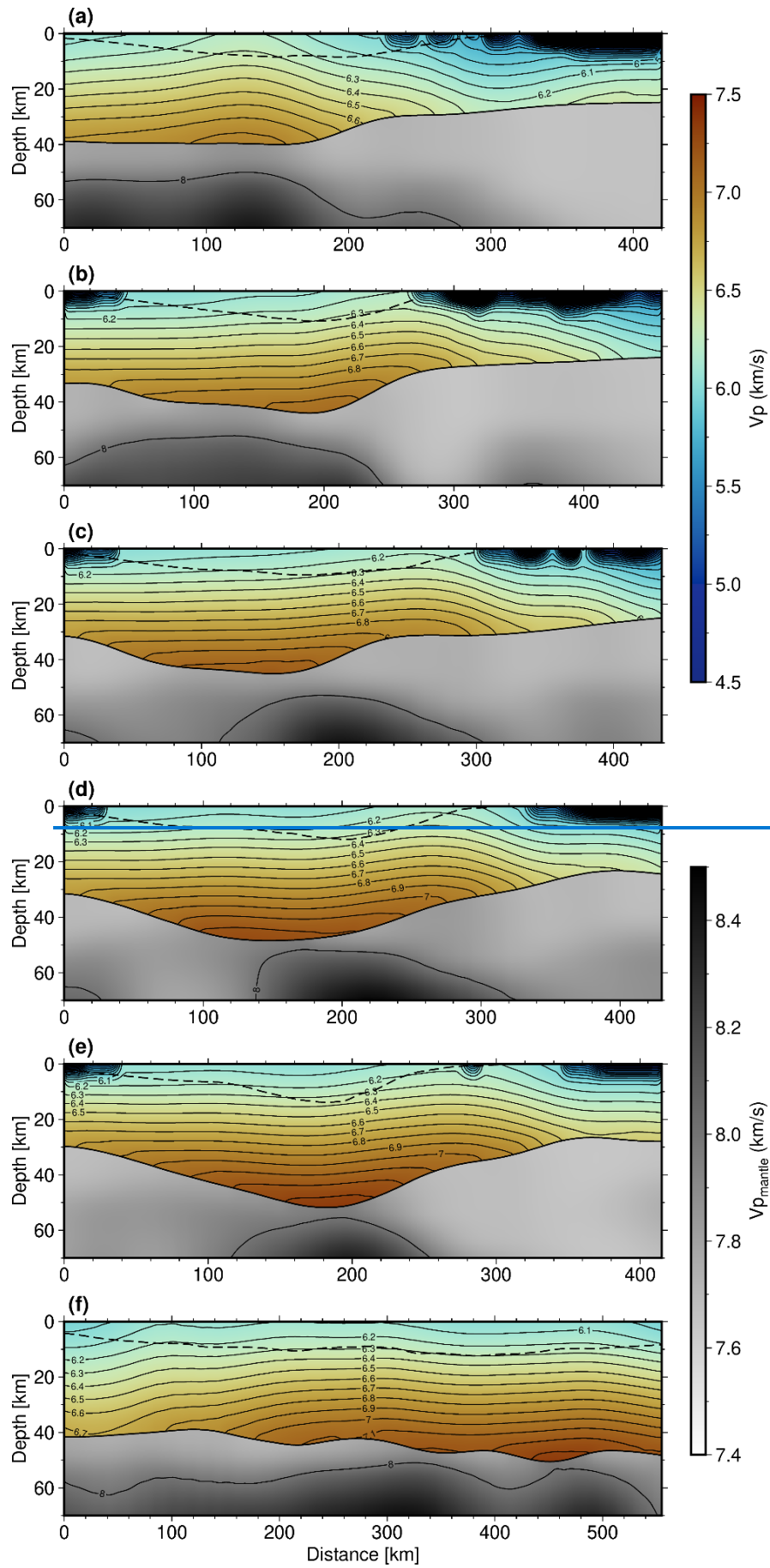
680 Profiles DD' and EE' (**Fig. 5d and 5e**) cross the southern part of the Dinarides. Here, the Moho reaches depths of over 50 km. Also, the crustal velocity at those depths ~~is the largest~~ **is the largest** of all the profiles, reaching almost 7.5 km/s. Greater Moho depths and crustal velocity change can be best seen in the profile FF' (**Fig. 5f**) running parallel to the Dinarides from northwest to southeast. In this profile Moho depth increases from around 40 km in the northern part to over 50 km in the southern part. Also, the crustal velocity just above Moho changes from just below 7.0 km/s in the north to almost 7.5 km/s in the south. Similarly, velocity in the mid-crustal zone (~20–25 km depth) is somewhat lower in the northern part of the profile, a little over 6.5 km/s, but becomes higher in the SE part reaching values of about 7 km/s.

690





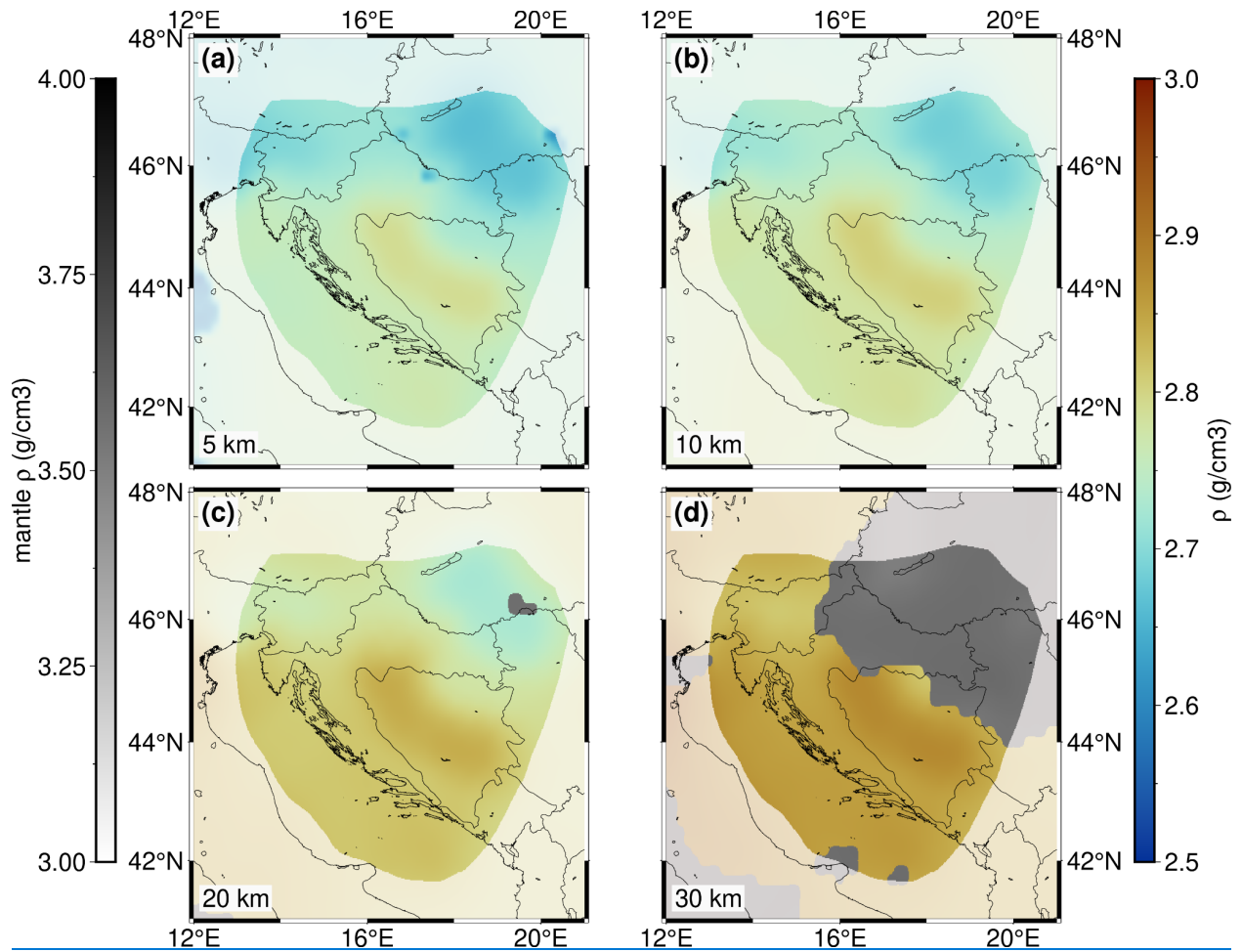


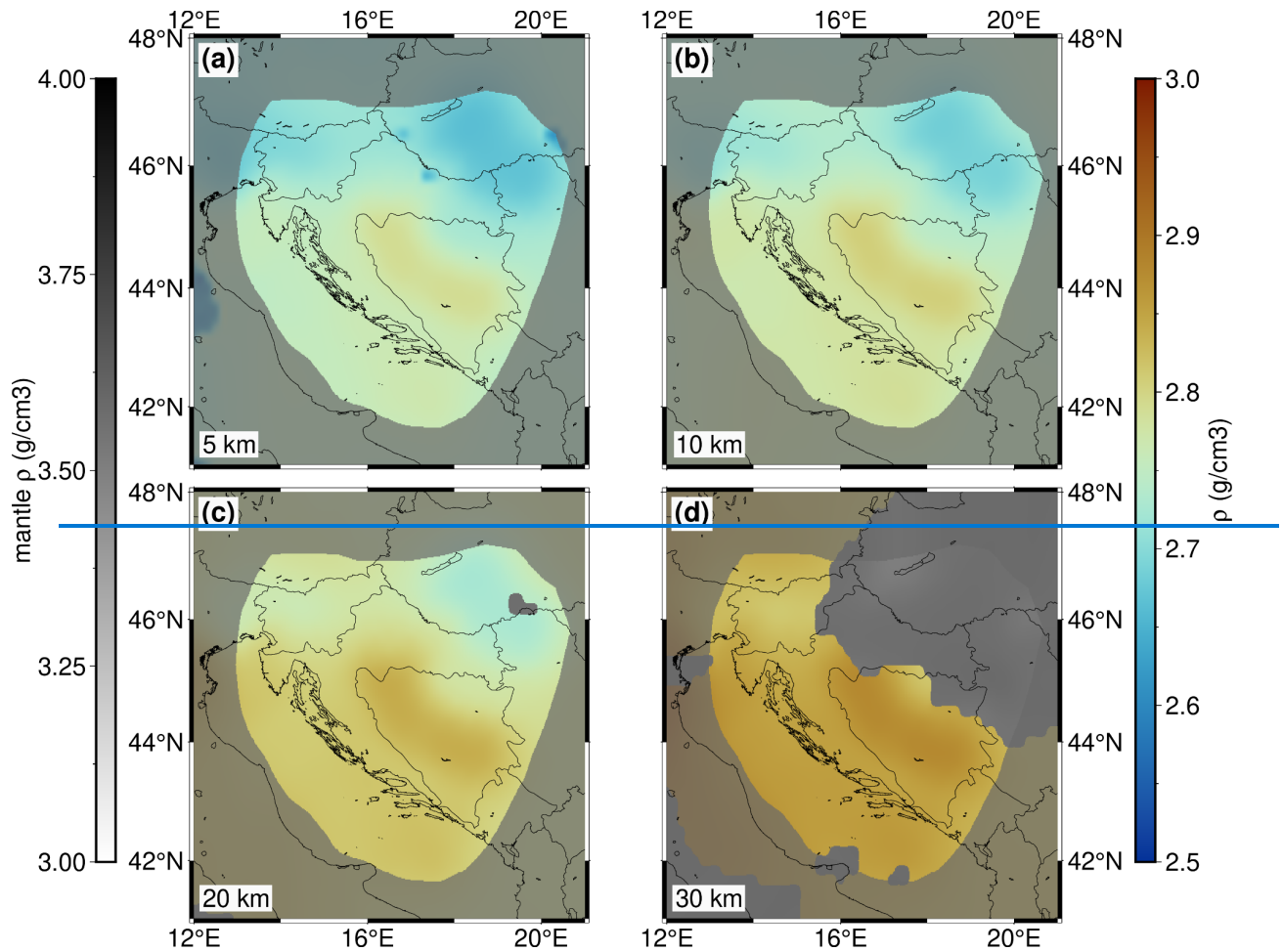


**Figure 5.** Profiles with locations shown in **Fig. 4cb**: (a) AA'; (b) BB'; (c) CC'; (d) DD'; (e) EE', and (f) FF'. Parallel full lines running approximately along the profile are the velocity isolinesgradient lines. The depth of the CRCCarbonate layer as derived from known geological data is indicated as the dashed line close to the surface.

~~As mentioned before it is interesting to note that the trend of velocity in the lower part of the crust corresponds to the velocity trends in the uppermost mantle. There is a positive velocity anomaly in the part of the uppermost mantle right below (or slightly offset from) the part of the crust with the deepest Moho. These positive anomalies in the work of Belinić et al. (2020) have been interpreted as a signal of the subducting Adria Microplate. Our model is mere interpolation of what was already known, but perhaps what we see here is part of the Adria crust being dragged along the uppermost part of the mantle being subducted below the Dinarides. As can be seen in the Fig. 5a, which is crossing into the SW Pannonian basin, the crustal velocity in that part is much lower than in the Dinarides, a feature also observed by Šumanovac et al. (2009). Perhaps the lower velocity is a feature of the Pannonian crust, whereas the relatively higher crustal velocity is a feature of the Adria crust. To make a definitive conclusion, more investigation should be performed.~~

From the smaller data set which includes the NAC model (Magrin and Rossi, 2020) and the gravimetric profiles (Šumanovac, 2010), we have interpolated the density values for the entire crust. The result is shown in **Fig. 6**. Keep in mind that for this interpolation there were only two sources of data, one of which had densities defined as isotropic layers (Šumanovac, 2010). Therefore, this parameter is much less accurate than P-wave velocity. As expected, this parameter reflects the results of Šumanovac (2010), since that was the main source of data. ~~It can be seen that the~~The density is slightly higher in the area of the Internal Dinarides than in the External Dinarides for all the depths considered here, possibly coinciding with higher density crystalline crust. In the SW Pannonian Basin the density has much lower values.



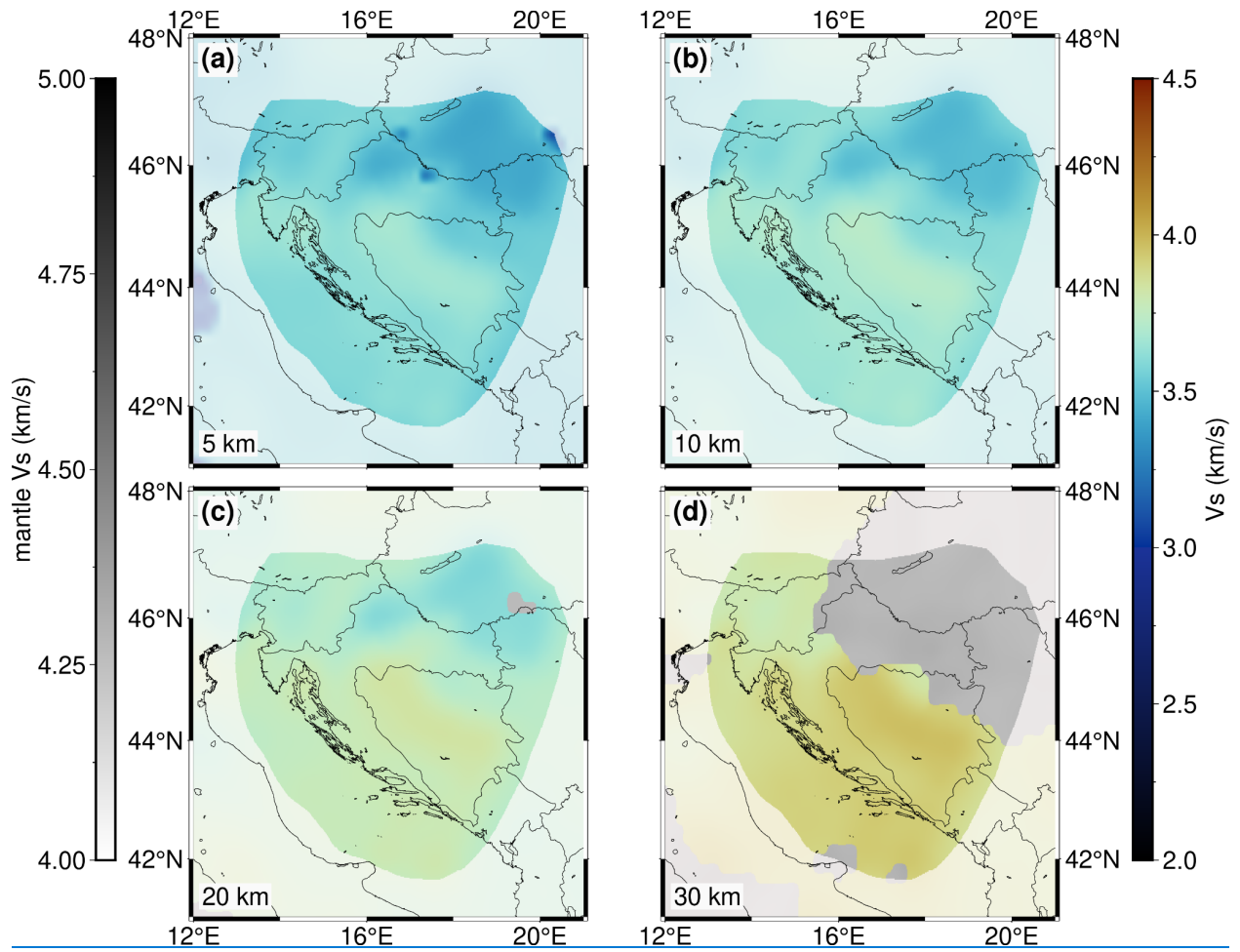


725 **Figure 6.** Density model depth slices for (a) 5 km, (b) 10 km, (c) 20 km, and (d) 30 km depth. The  
 730 areas of lower resolution are shaded and the gray color scale corresponds to the mantle density  
 735 (see text for details)  
 740

**Fig. 7** shows the S-wave velocity at four depths. In this case, there was no measured S-wave velocity data (the only available  $V_s$  results were from the NAC model which covers the

western corner of our study area) so these values were estimated using the P-wave velocity and Brocher's (2005) empirical relation.

745





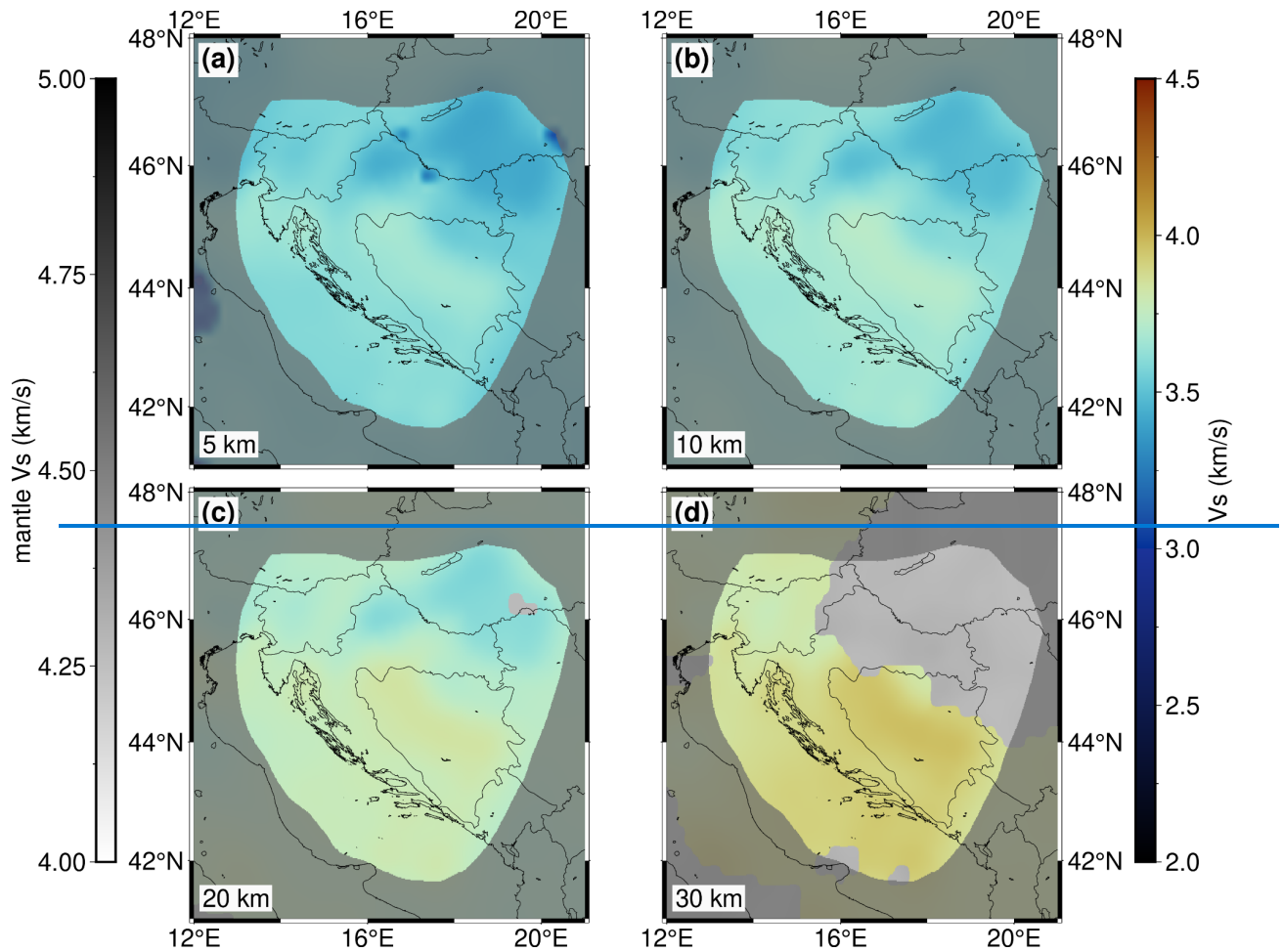


**Figure 7.** S-wave velocity depth slices for (a) 5 km, (b) 10 km, (c) 20 km, and (d) 30 km depth. The areas of lower resolution and the gray color scale corresponds to the mantle velocity (see text for details).

## Discussion

755 The creation of the presented 3-D model was inspired by the need for the more complete seismic model of the Dinarides. Although there have been previous studies estimating various properties of the crust in the region, the complete seismic model of the Dinarides crust and upper mantle ~~did still does~~ not exist ~~until this study~~. In this study we assembled data from previous ~~investigationsstudies~~ to create a first comprehensive model of the crust for the wider Dinarides area. Moho depth is the best constrained parameter of our model, since there were ~~several good sources of enough~~ high-quality data regarding this parameter. ~~It confirms what we already know about Moho in the Dinarides, but now it is presented as a comprehensive, ready-to-use model. It is mainly based on Stipčević et al. (2020) study and our model reflects all the features noted therein. As shown in Fig. 5f the Moho deepens going from the NW to the SE along the main axis of the Dinarides. Also, from the profiles in Figs. 5a-e it can be seen that the change in Moho depth going from the Adriatic Sea towards the Dinarides mountain chain is much more gradual than on the other side, going from the Dinarides towards the SW Pannonian basin, where this change is much more abrupt, almost step-like. The same feature has been observed by Šumanovac et al. (2009) and Šumanovac (2010).~~

760 ~~In the case of Neogene deposits thickness the data used came from two sources (Saftić et al., 2003 and Matenco and Radivojević, 2012), and they provided adequate coverage in the area of the SW Pannonian Basin where the thick Neogene deposits are located.~~

770 For the Neogene deposit thickness, we used manually digitized maps, therefore having less precise data, ~~but which were originally created from a high number of active seismic profiles and thus strengthening our confidence that~~-this parameter was adequately presented in our model. The thickest Neogene sedimentary cover can be found in the area of the Sava and Drava depressions with thinner cover in the rest of the SW Pannonian basin and almost non-existent in other regions, most notably in the Dinarides, as well as in some hilly areas of the SW Pannonian Basin.

780 For P-wave velocity, ~~the most valuable data available were the seismic refraction/reflection profiles (Brückl et al., 2007; Šumanovac et al., 2009) and the high-quality NAC model (Magrin and Rossi, 2020).~~As can be seen in **Fig. 1**, all the ~~P-wave velocity~~ high-quality data are concentrated in the NNW part of the study area. In the southern part, we relied on the inverted gravimetric profile data (Šumanovac, 2010), which is not the ideal data source due to the high uncertainties and lower resolution. Nevertheless, given the lack of other data sources for South Dinarides, even the data from the gravimetric profiles proved to be of high value. ~~It seems that the velocity in the Internal Dinarides, where we only had inverted gravimetric profile data available, is slightly higher than in the rest of the model. At this point, we cannot discern if it is an actual feature, or some artifact due to lower quality data. The~~

785

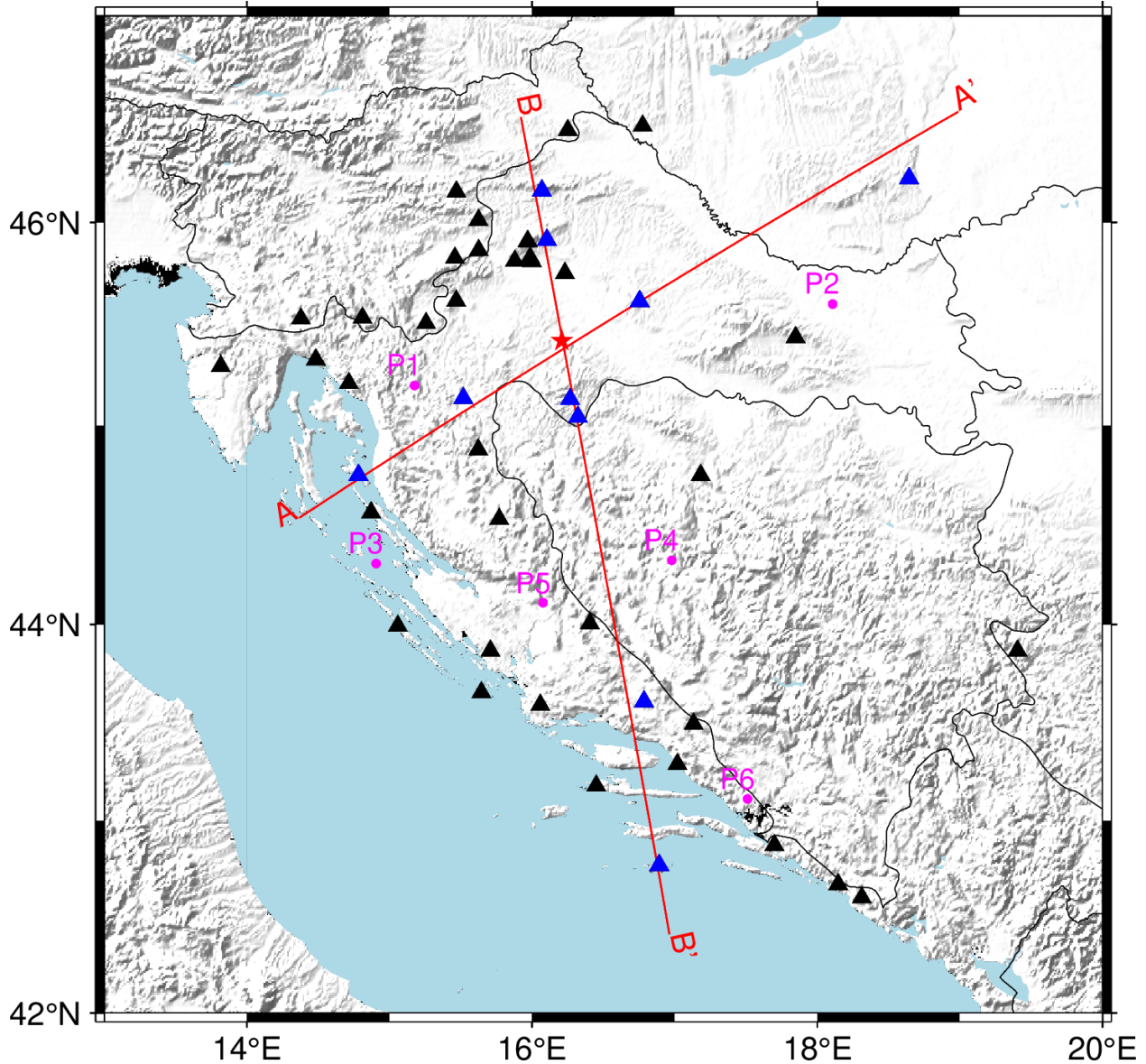
790 [fact is that this is a different tectonic unit, so it is not impossible that it has different features.](#)  
795 [If we have omitted these data from interpolation, we would have even worse results, because](#)  
[in that case the values would be purely extrapolated. The approach we chose gave at least](#)  
[some constraint to the velocity values in this part of the model. In the Fig. 5a, the](#)  
[northernmost profile shows the similar features as the profile interpreted by Šumanovac et](#)  
[al. \(2009\) — the crustal velocity in the SW Pannonian Basin is much lower than in the](#)  
[Dinarides. The other profiles, located further south, also cutting across the Internal](#)  
[Dinarides, show that the crustal velocity in the Internal Dinarides, is generally a bit higher](#)  
[than in the External Dinarides with relatively quick transition to the lower seismic velocity](#)  
[values in the Pannonian basin \(see profiles CC', DD' and EE'\).](#)

800 [It is interesting to note that the trend of velocity in the lower part of the crust corresponds](#)  
[to the velocity trends in the uppermost mantle. There is a positive velocity anomaly in the](#)  
[part of the uppermost mantle right below \(or slightly offset from\) the part of the crust with](#)  
[the deepest Moho. These positive anomalies in the work of Belinić et al. \(2020\) have been](#)  
[interpreted as a signal of the subducting Adria Microplate. Our model is mere interpolation](#)  
[of what was already known, but perhaps what we see here is part of the Adria crust being](#)  
805 [dragged along with the uppermost part of the mantle in the subduction below the Dinarides.](#)  
[As can be seen in the Fig. 5a, which is crossing into the SW Pannonian basin, the crustal](#)  
[velocity in that part is much lower than in the Dinarides, a feature also observed by](#)  
[Šumanovac et al. \(2009\). Perhaps the lower velocity is a feature of the Pannonian crust,](#)  
[whereas the relatively higher crustal velocity is a feature of the Adria crust. To make a](#)  
810 [definitive conclusion, more investigation should be performed.](#)

The velocity estimation for the Neogene deposits and the Mesozoic carbonates proved particularly challenging since there is little available data about this parameter. In the case of Neogene deposits, we used Brocher's (2008) relation for the deposits of similar age. For the ~~CRC~~carbonate layer, we could not derive any velocity–depth relation due to the lack of  
815 available data, so in this case, we simply used the same velocity interpolation as for the rest of the crust. It seems, though, that at least in some parts of our new model, the ~~CRC~~Carbonate bottom depth coincides with the velocity of around 6.2 - 6.35 km/s.

To test how well the newly derived 3-D model represents the true structure, we calculated the travel times for a regional earthquake recorded on representative seismic stations in the wider Dinarides area (**Fig. 8**). We also calculated travel times using the simple 1D model with two isotropic crust layers currently employed for routine earthquake locating in Croatia  
820 ([B.C.I.S. \(1972\)](#), [Herak et al., 1996](#)). The 1D model's topmost layer is characterized by P-velocity of 5.8 km/s, and the deeper crustal layer has the P-wave velocity of 6.65 km/s. For the same model the uppermost mantle velocity is 8.0 km/s. We then compared the travel  
825 times from both models with the true measured travel times. We used the Pn and Pg phases of the 2020 Petrinja Mw6.4 earthquake. The location of the earthquake ([42.4188°N, 16.2082](#)

830 | [°E, 7.57 km](#)) and the stations that recorded the wave onsets are shown in **Fig. 8**. For the same stations we calculated the travel times using the 1D and the new 3-D model. For travel time calculation we used the Fast Marching Method (de Kool et al., 2006) as implemented within the FMTOMO package (Rawlinson and Urvoy, 2006).



835 **Figure 8.** A map showing the epicenter of the Petrinja 2020 earthquake sequence mainshock (red star) and stations we used for calculation of traveltimes (black and blue triangles). Travel times for all the stations are shown in **Figs. 9** and **10**. The red lines mark the positions of the cross sections shown in **Fig. 11** (section AA') and **Fig. 12** (section BB'). The stations coloured blue are the ones shown in **Fig. 11** and **Fig. 12**. The points coloured in magenta mark the position of 1D models shown in **Fig. 13**.

Calculated travel times are shown in **Figs. 9** and **10**, for Pg and Pn phase, respectively. Figures show the differences in travel times calculated [between](#) the models (both 1D and 3-D) and observed travel times. When looking at Pg phases (**Fig. 9**), we can see improvement in calculated travel time accuracy when using the 3-D model [\(with respect to the 1-D model\)](#) for epicentral distances smaller than 50 km and over 100 km. For smaller epicentral distances, the more accurate travel times in the 3-D model are connected with better specification of Neogene sedimentary cover with low P-wave velocity. On the other hand, for epicentral distances between 50 and 80 km 1D and 3-D models travel times are similarly offset compared to the observed travel times, with times calculated using the 1D model being slightly more accurate. We believe this is due to the less accurate velocity sampling in the upper crust in the transitional zone between Internal Dinarides and [SW Pannonian Basin](#) and lack of knowledge about spatial coverage of the [CRC Carbonate complex layer](#) in this area. For greater epicentral distances we can see that travel times calculated using the 3-D model are much more accurate compared to those calculated using the 1D model. That means that the crustal velocity derived in our 3-D model is a considerable improvement of the simple 1D model.

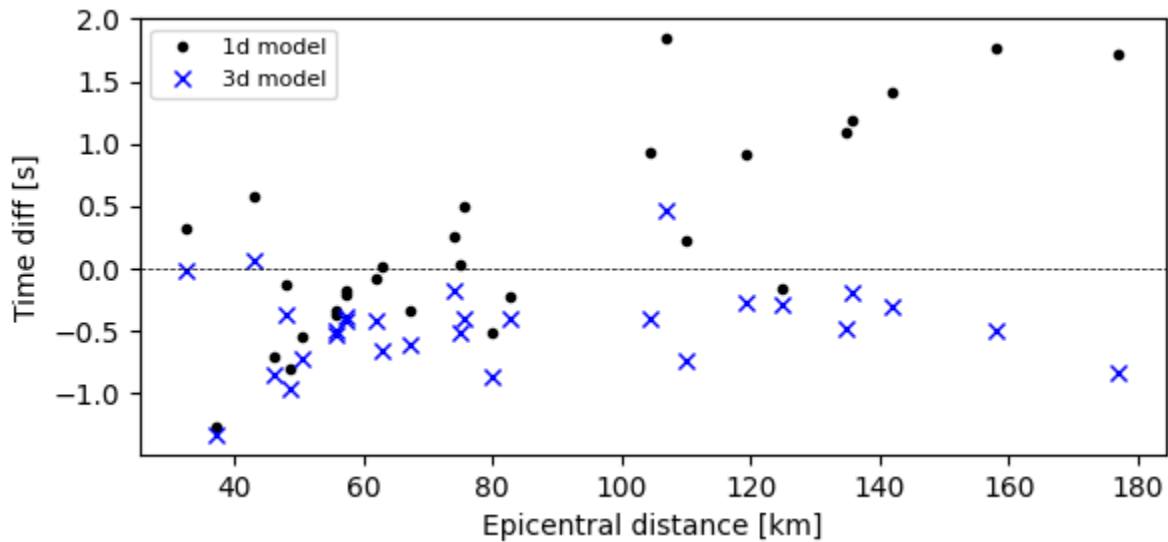


**Figure 9.** Pg phase travel times for the 2020 Petrinja earthquake: time difference between 1D model and observed travel times (black dots) and between 3-D model and observed travel times (blue crosses).

Concerning the Pn phases (**Fig. 10**), we can see that the travel times calculated using the 3-D model are generally closer to the actual observed travel times for all the epicentral distances shown than those calculated using the 1D model. In case of Pn phases, the uppermost mantle velocity plays a great part in the total travel times, so both the crustal model we derived here and the mantle model from Belinić et al. (2020) show improvement compared to the 1D model. There is still room for improvement in the uppermost mantle



865 | velocity, since the model of Belinić et al. (2020) we used here is most accurate for greater depths (80–100 km).

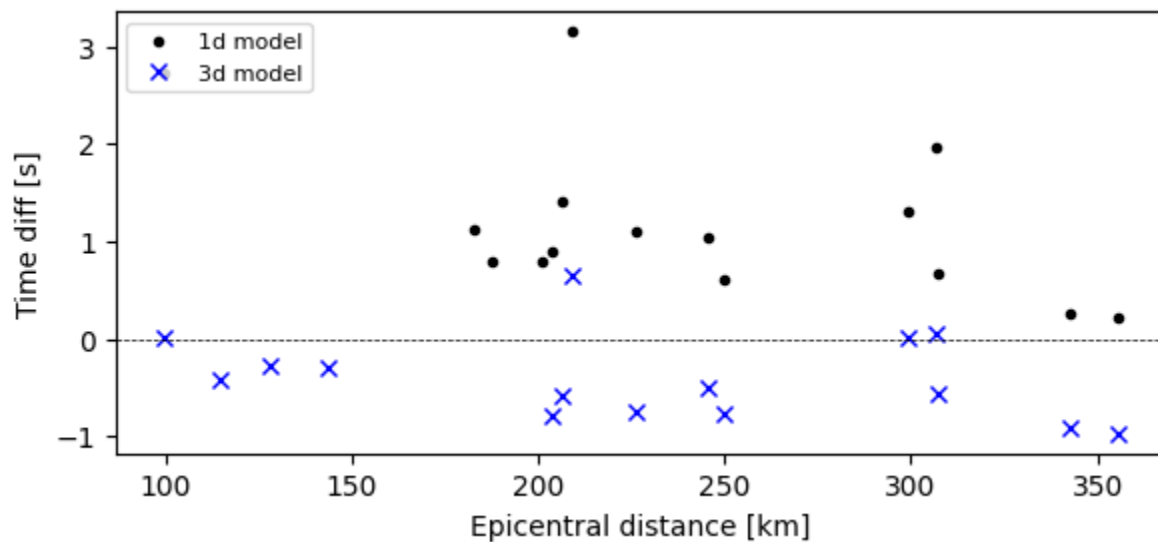


**Figure 10.** Pn phase travel times for the 2020 Petrinja earthquake: time difference between 1D model and observed travel times (black dots) and between 3-D model and observed travel times (blue crosses).

870 **Figure 11** shows a cross section AA' (from **Fig. 8**) of the newly derived 3-D model, with the  
calculated ray paths using the simple 1D and 3-D models. The section was chosen in a way  
to show travel times for both Pg and Pn phases, and -we also tried to position it in such a way  
that it crosses almost perpendicularly the main strike of the Dinarides. There is also another  
cross section shown in **Fig. 12** (BB'), oriented approximately north to south. Position of the  
875 stations shown in cross section BB' is also marked in **Fig. 8**. From both profiles it can be seen  
that the seismic rays cover completely different paths depending on whether they were  
calculated using the 1D or the 3-D model. For example, the Pg phases, when calculated using  
the 3-D model, travel much deeper than their 1D counterparts. Also, since the Moho in the  
Pannonian Basin of our 3-D model is much shallower than the Moho in the simple 1D model,  
880 the calculated rays using either 1D or 3-D model travel on very different paths in the  
uppermost mantle. That is particularly visible in **Fig. 12**, in case of the ray path between the  
source and the most distant station shown. The ray path calculated for the 3-D model reaches  
depths of almost 60 km, while the same ray path calculated for the 1D model reaches depths  
of only 40 km, which is a huge difference. Given all that, it can be concluded that precise  
885 knowledge about the crustal model is very important for all seismic applications.



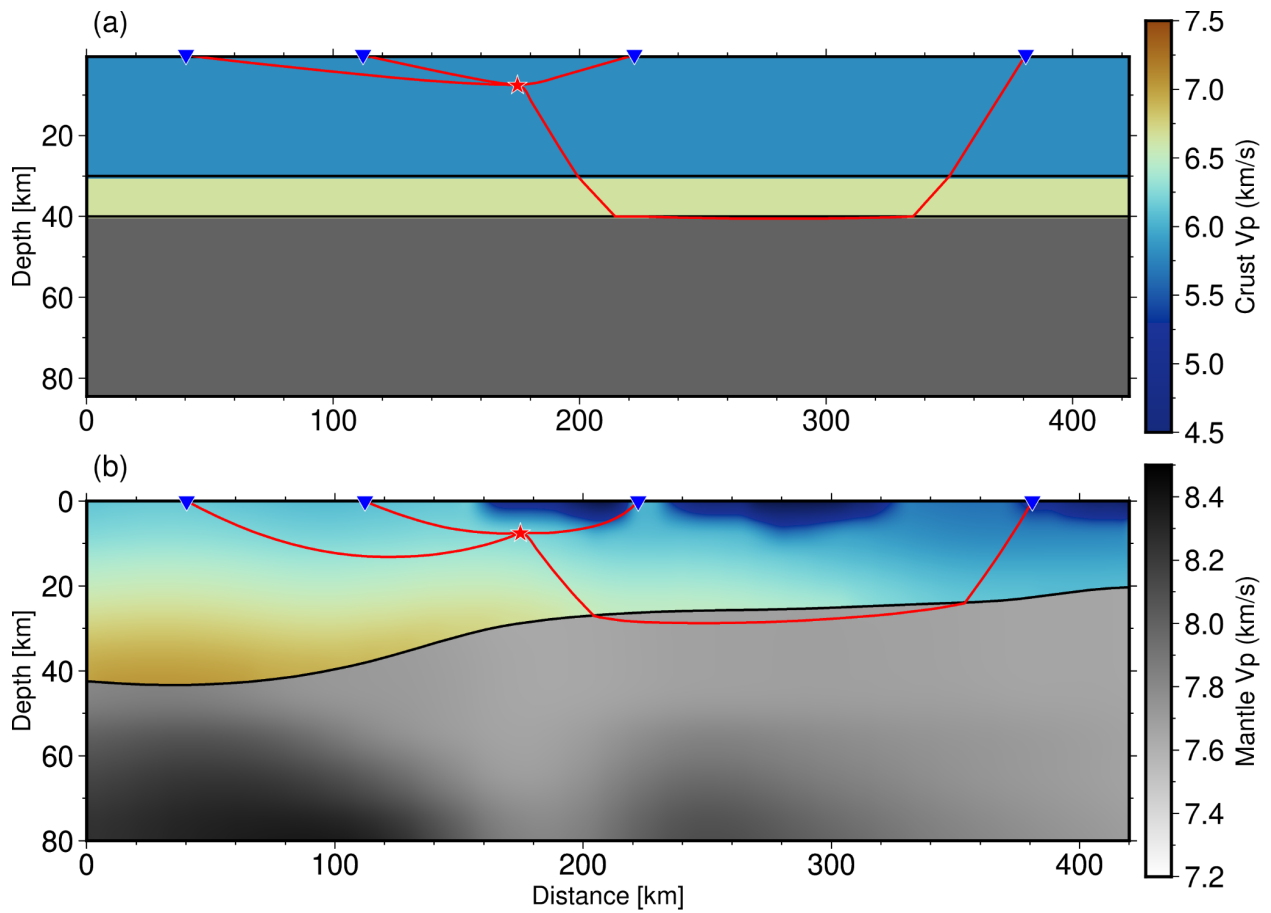


**Figure 11.** Earthquake ray paths in cross section AA' (for location see **Fig. 8**) for two models: (a) a simple 1D model with two isotropic crustal layers, and (b) our 3-D model with one anisotropic crustal layer. Colorbars are the same for both panels.

890

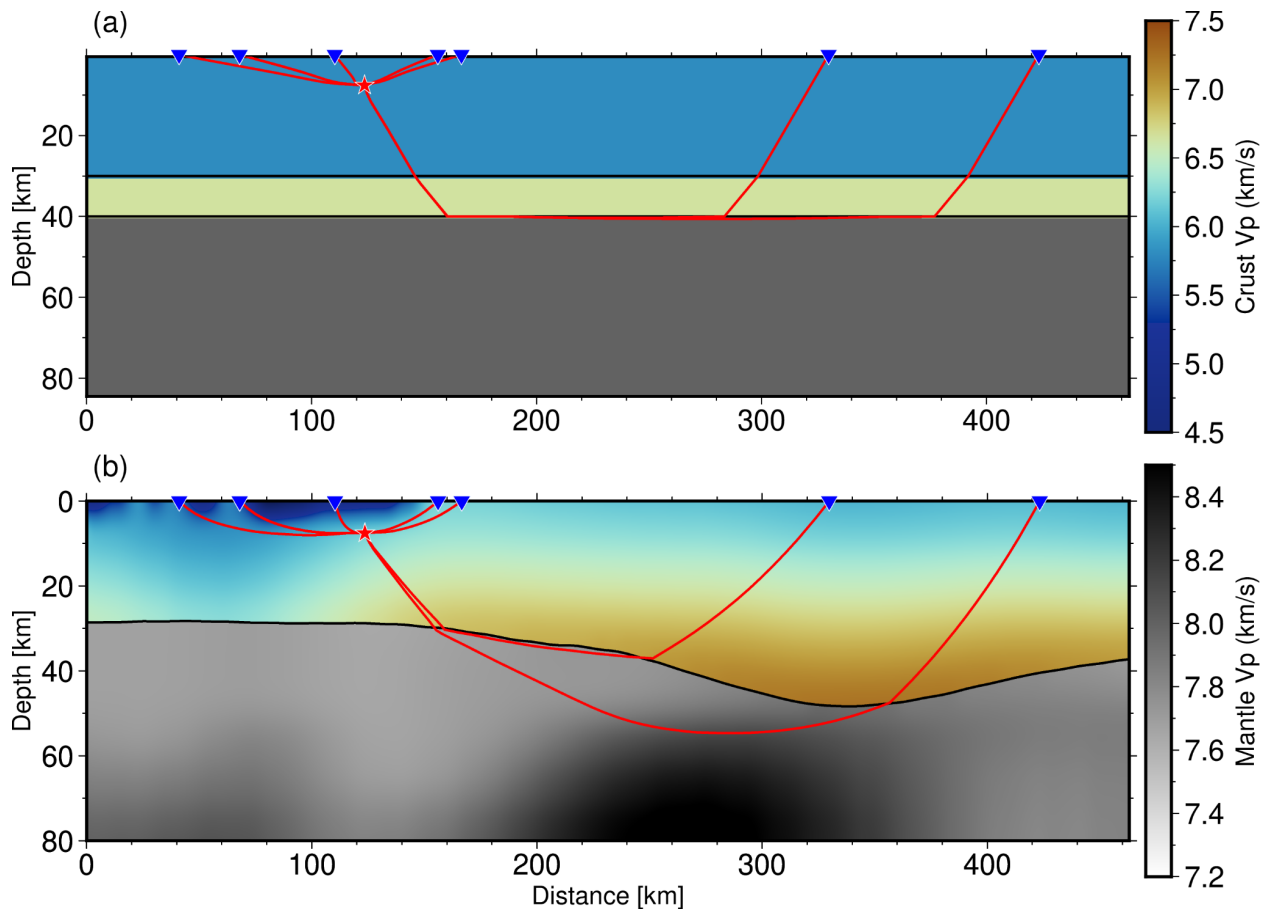
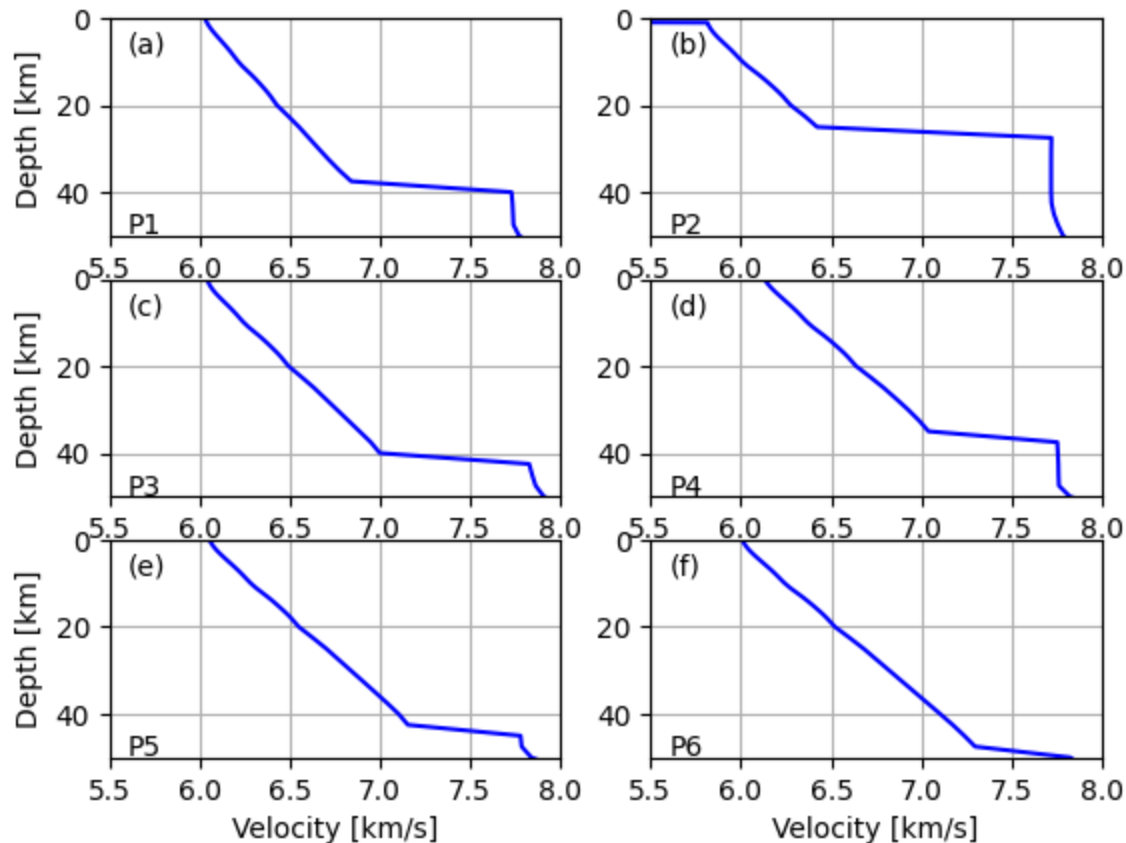


**Figure 12.** Earthquake ray paths in cross section BB' (for location see **Fig. 8**) for two models: (a) a simple 1D model with two isotropic crustal layers, and (b) our 3-D model with one anisotropic crustal layer. Colorbars are the same for both panels.

895

In addition to the profiles shown in **Figs. 11** and **12**, we have also extracted 1D depth velocity models for six points marked in **Fig. 8** in magenta. Those six points have been chosen to cover different domains of our model (Stable Adria, Internal and External Dinarides, and the SW Pannonian Basin). The velocity change with depth for the chosen six points is shown in **Fig. 13**. For example, at the P2 point, which is located in the SW Pannonian Basin, the velocity for the first couple of kilometers of depth is much lower than for the other points because there is a Neogene deposits layer on top. The outlook of each model shown in **Fig. 13** is generally similar at each point with obvious differences being Moho depth (see points P2 and P1) and rate of increase of velocity with depth (e.g., compare points P3 and P5).

900



905

**Figure 13.** Velocity changes with depth for six points (P1 to P6; for locations see **Fig. 8**).

## Conclusions

Having a complete 3-D model of the crustal structure is a major step forward in the study of the Dinarides and the surrounding areas. The newly derived model is defined on a regular dense grid for three key parameters (P- and S-velocity and density), and as such can be readily used by seismologists who need information on crustal structure as input for their studies (earthquake locating, seismic tomography, shaking estimation, seismic hazard...). We tested the performance of the model in comparison with the commonly used 1D model and found significant improvements in time travel calculations. The model still has some inherent weaknesses that have been discussed in the previous sections which are mostly connected with low number of measurements in some parts of the region. Nevertheless, the 3-D model represents a good first step towards improving the knowledge of the crustal structure in the complex area of the Dinarides.

920

925 The model clearly delimits several key areas (Dinarides, Pannonian Basin and Adriatic Sea) as well as distinguishing distinct layers in those that regions (i.e., Neogene deposits and Carbonates). The most robust feature of the model is the depth to Mohorovičić discontinuity, but other parameters are also reasonably well defined. Inclusion of the Carbonate complex thickness is, to the best of our knowledge, the first attempt to estimate this parameter for the whole Dinarides region. One of the new insights found during the creation of the model is the relatively high (P-wave) velocity for the lower crust in the southern part of the Dinarides. This feature needs to be confirmed by other studies, given 930 the sparsity of information about velocity for that region. On the other hand, the high velocity feature fits nicely to the higher velocity of the uppermost mantle found in the same area thus corroborating the idea of continental subduction (and/or lithospheric delamination) in south-central External Dinarides.

935 In conclusion, the model presented here represents the currently best and most complete crustal model for the wider Dinarides region. Model is assembled from all the available measurements on seismic velocity, density, layer composition and thickness to provide a full representation of the major variations of seismic wavespeeds in the regional crust. Hopefully, the new 3-D model will help discover some new, previously unknown features of the crust and in turn, each new study that sheds some light on the crustal structure in this 940 area may improve the 3-D model derived here.

## Resources

The model derived in this work is available on the following link:  
<https://urn.nsk.hr/urn:nbn:hr:217:793485>

## Acknowledgements

945 This work has been supported in part by the Croatian Science Foundation under the Project No. IP-2020-02-3960. This research was performed using the resources of computer cluster Isabella based in SRCE – University of Zagreb University Computing Centre. We thank professor Marijan Herak for the review and comments which helped us improve this manuscript.

950

## References

Aljinović, B.: Najdublji seizmički horizonti sjeveroistočnog Jadrana, Ph. D. thesis (in Croatian with English abstract), University of Zagreb, Croatia, 219 pp., 1983.

955 Aljinović, B., Prelogović, E., and Skoko, D.: New data on deep geological structure and seismotectonic active zones in region of Yugoslavia, *Boll. di Oceanol. Teorica ed Applicata*, 2, 77–90, 1987.

960 Artemieva, Irina M., and Thybo, H.: EUNaseis: A seismic model for Moho and crustal structure in Europe, Greenland and the North Atlantic region, *Tectonophysics*, 609, 97–105, doi:<http://dx.doi.org/10.1016/j.tecto.2013.08.004>, 2013.

Balling, P., Tomljenović, B., Schmid, S. M., and Ustaszewski, K.: Contrasting along-strike deformation styles in the central external Dinarides assessed by balanced cross-sections: implications for the tectonic evolution of its Paleogene flexural foreland basin system, *Global Planetary Change*, 205, 103587, <https://doi.org/10.1016/j.gloplacha.2021.103587>, 2021.

965 B. C. I. S. (1972): Tables des temps des ondes séismiques. Hodochrones pour la region des Balkans (Manuel d'utilisation). Strasbourg.

970 Belinić, T., Stipčević, J., Živčić, M., and the AlpArrayWorking Group: ~~(2018)~~ Lithospheric thickness under the Dinarides, *Earth and Planetary Science Letters*, 484, pp 229–240, doi:<https://doi.org/10.1016/j.epsl.2017.12.030><https://doi.org/10.1016/j.epsl.2017.12.030>, 2018.

Belinić, T., Kolínský, P., Stipčević, J., and AlpArray Working Group: ~~(2020)~~ Shear-wave velocity structure beneath the Dinarides from the inversion of Rayleigh-wave dispersion, *Earth and Planetary Sciences Letters*, 555, <https://doi.org/10.1016/j.epsl.2020.116686>, 2020.

975 Brocher, T. M.: ~~(2005)~~ Empirical relations between elastic wavespeeds and density in the Earth's crust, *Bulletin of the Seismological Society of America*, Vol 95/, No. 6, pp 2081–2092. <https://doi.org/10.1785/0120050077>, 2005.

980 Brocher, T. M.: ~~(2008)~~ Compressional and Shear-Wave Velocity versus Depth Relations for Common Rock Types in Northern California, *Bulletin of the Seismological Society of America*, Vol. 98/, No. 2, pp 950–968. doi: 10.1785/0120060403, 2008.

Brückl, E., Bleibinhaus, F., Gosar, A., Grad, M., Guterch, A., Hrubcová, P., Keller, G. R., Majdański, M., Šumanovac, F., Tiira, T., Yliniemi, J., Hegedus, E., and Thybo, H.: ~~(2007)~~ Crustal structure due to collisional and escape tectonics in the Eastern Alps region based on profiles

Alp01 and Alp02 from the ALP 2002 seismic experiment. *Journal of Geophysical Research*,  
985 ~~Vol.~~ 112, B06308, doi:10.1029/2006JB004687, [2007](https://doi.org/10.1029/2006JB004687)

Cloetingh, S., Bada, G., Matenco, L., Lankreijer, A., Horvath, F., and Dinu, C.: ~~(2006)~~. Modes of  
basin(de)formation, lithospheric strength and vertical motions in the Pannonian–Carpathian  
system: inferences from thermo-mechanical modeling. *Geological Society, London, Memoirs*,  
990 ~~Vol.~~ \_\_\_\_\_ 32, \_\_\_\_\_ 207–221,  
<https://doi.org/10.1144/GSL.MEM.2006.032.01.12><https://doi.org/10.1144/GSL.MEM.2006.032.01.12>, 2006

Csontos, L., and Vörös, A.: ~~(2004)~~. Mesozoic plate tectonic reconstruction of the Carpathian  
region. *Palaeoclimatology, Palaeoecology, Palaeogeography*, 210, 1–56,  
995 <https://doi.org/10.1016/j.palaeo.2004.02.033>, [2004](https://doi.org/10.1016/j.palaeo.2004.02.033)

Cvetko Tešović, B., Martinuš, M., Golec, I., and Vlahović, I.: ~~(2020)~~. Lithostratigraphy and  
biostratigraphy of the uppermost Cretaceous to lowermost Palaeogene shallow-marine  
succession: top of the Adriatic Carbonate Platform at the Likva Cove section (island of Brač,  
Croatia). *Cretaceous Research*, 114, 104507,  
1000 <https://doi.org/10.1016/j.cretres.2020.104507>, 2020.

de Kool, M., Rawlinson, N., and Sambridge, M.: ~~(2006)~~. A practical grid-based method for  
tracking multiple refraction and reflection phases in three-dimensional heterogeneous  
media. *Geophys. J. Int.*, 167, 253270. doi: 10.1111/j.1365-246X.2006.03078.x, [2006](https://doi.org/10.1111/j.1365-246X.2006.03078.x)

Dragašević, T., and Andrić, B.: ~~(1975)~~. Dosadašnji rezultati ispitivanja građe Zemljine kore  
dubokim seizmičkim sondiranjem na području Jugoslavije *(in Serbian)*. *Acta Seismologica*  
1005 *Iugoslavica*, 2–3, 47–50, [1975](https://doi.org/10.1016/j.cretres.2020.104507). *(in Serbian)*

Fodor, L., Jelen, B., Márton, E., Skaberne, D., Čar, J., and Vrabec, M.: ~~(1998)~~. Miocene–Pliocene  
tectonic evolution of the Slovenian Periadriatic fault: implications of Alpine–Carpathian  
extrusion models. *Tectonics*, 17, 690–709, <https://doi.org/10.1029/98TC01605>, 1998.

Frisch, W., Kuhlemann, J., Dunkl, I., and Brugel, A.: ~~(1998)~~. Palinspastic reconstruction and  
topographic evolution of the Eastern Alps during late Tertiary tectonic extrusion.  
1010 *Tectonophysics*, 297, 1–15, [https://doi.org/10.1016/S0040-1951\(98\)00160-7](https://doi.org/10.1016/S0040-1951(98)00160-7)  
[https://doi.org/10.1016/S0040-1951\(98\)00160-7](https://doi.org/10.1016/S0040-1951(98)00160-7), 1998.

[Geological Map of Albania 2002: Geological 1 : 200 000 map published by the Ministry of  
Industry & Energy and the Ministry of Education & Science, Tirana.](#)

Grad, M., Tiira, T., and ESC Working Group: ~~(2009)~~. The Moho depth map of the European  
Plate. *Geophys. J. Int.*, 176, pp. 279–292. <https://doi.org/10.1111/j.1365-246X.2008.03919.x>, 2009.



- 1020 ~~Handy, M. R., Schmid, S. M., Bousquet, R., Kissling, E., and Bernoulli, D. (2010). Reconciling plate tectonic reconstructions of Alpine Tethys with the geological–geophysical record of spreading and subduction in the Alps. *Earth Science Reviews* 102, 121–158. <https://doi.org/10.1016/j.earscirev.2010.06.002>~~
- Handy, M. R., Giese, J., Schmid, S. M., Pleuger, J., Spakman, W., Onuzi, K., and Ustaszewski, K.: ~~(2019)~~. Coupled crust-mantle response to slab tearing, bending and rollback along the Dinaride–Hellenide orogen. *Tectonics*, 38, 2803–2828, <https://doi.org/10.1029/2019TC005524>, 2019.
- ~~Herak, M., Herak, D. and Markušić, S. (1996): Revision of the earthquake catalogue and seismicity of Croatia, 1908–1992, *Terra Nova*, 8, 86–94.~~
- Horváth, F., Bada, G., Szafián, P., Tari, G., Ádám, A., and Cloetingh, S. ~~(2006)~~: Formation and deformation of the Pannonian basin: constraints from observational data. In: ~~Gee, D.G., Stephenson, R.A. (Eds.)~~, *European Lithosphere Dynamics*, edited by ~~Gee, D.G., Stephenson, R.A. (Eds.)~~, Memoirs, Geological Society, London, Vol.—32, 191–206, <https://doi.org/10.1144/GSL.MEM.2006.032.01.11><https://doi.org/10.1144/GSL.MEM.2006.032.01.11>, 2006
- 1030
- Kapuralić, J., Šumanovac, F., and Markušić, S.: ~~(2019)~~. Crustal structure of the northern Dinarides and southwestern part of the Pannonian basin inferred from local earthquake tomography. *Swiss Journal of Geosciences* 112, pp—181–198. doi: <https://doi.org/10.1007/s00015-018-0335-2>, 2019
- 1035
- ~~Kennett, B., Engdahl, E., and Buland, R. (1995). Constraints on seismic velocities in the Earth from traveltimes. *Geophys. J. Int* 122, 108–124. doi: <https://doi.org/10.1111/j.1365-246X.1995.tb03540.x>~~
- 1040
- ~~Kerbar, T. (2009). Orogenic evolution of the External Dinarides in the NE Adriatic region: a model constrained by tectonostratigraphy of Upper Cretaceous to Paleogene carbonates. *Earth Science Reviews* 96, 296–312. <https://doi.org/10.1016/j.earscirev.2009.07.004>~~
- 1045
- Magrin, A., and Rossi, G.: ~~(2020)~~. Deriving a new crustal model of Northern Adria: The Northern Adria crust (NAC) model. *Frontiers in Earth Science*, 8:89. <https://doi.org/10.3389/feart.2020.00089>, 2020.
- Matenco, L., and Radivojević, D.: On the formation and evolution of the Pannonian Basin: Constraints derived from the structure of the junction area between the Carpathians and Dinarides, *Tectonics*, 31, TC6007, <https://doi.org/10.1029/2012TC003206>, 2012.
- 1050
- Mohorovičić, A.: ~~(1910)~~. Potres od 8. X. 1909., Godišnje izvješće zagrebačkog meteorološkog opservatorija, 9(4/1), 1–56, 1910.

- Molinari, I., and Morelli, A.:~~(2011)~~. EPcrust: a reference crustal model for the European Plate. *Geophys. J. Int.*, 185, 352–364, <https://doi.org/10.1111/j.1365-246X.2011.04940.x>, 2011
- 1055 Olea, R. A.:~~(1999)~~. Geostatistics for engineers and Earth scientists. Springer Science + Business Media, New York, 320 pp., ISBN 978-0792385233, 1999.
- Orešković, J., Šumanovac, F., and Hegedüs, E.:~~(2011)~~. Crustal structure beneath the Istra peninsula based on receiver function analysis. *Geofizika*, Vol. 28, 247–263, 2011.
- 1060 [Osnovna Geološka Karta SFRJ: Geological maps of former Yugoslavia, 1 : 100.000, Beograd, Savezni Geoloski Zavod.](#)
- Pebesma, E. J.:~~(2004)~~. “Multivariable geostatistics in R: the gstat package”. *Computers & Geosciences*, 30, 683–691. <https://doi.org/10.1016/j.cageo.2004.03.012>, 2004.
- 1065 Rawlinson, N., and Urvoy, M.:~~(2006)~~. Simultaneous inversion of active and passive source datasets for 3-D seismic structure with application to Tasmania. *Geophys. Res. Lett.*, 33, <https://doi.org/10.1029/2006GL028105>, 2006.
- Ratschbacher, L., Merle, O., Davy, P., and Cobbold, P. :~~(1991a)~~. Lateral extrusion in the Eastern Alps, Part 1: Boundary conditions and experiments scaled for gravity. *Tectonics*, Vol. 10/, No. 2, 245–256, <https://doi.org/10.1029/90TC02622>, 1991a
- 1070 Ratschbacher, L., Frisch, W., Linzer, H.-G., and Merle, O.:~~(1991b)~~. Lateral extrusion in the Eastern Alps, Part 2: Structural analysis. *Tectonics*, 10, 257–271, <https://doi.org/10.1029/90TC02623><https://doi.org/10.1029/90TC02623>, 1991b
- Royden, L. H., and & Horváth, F.:~~(1988)~~. The Pannonian Basin -- A study in basin evolution. [edited by](#) Royden, L. H., and & Hórvath, F.:~~(Eds.)~~. AAPG Memoirs, 45, The American Association of Petroleum Geologists Tulsa, Oklahoma (USA) & Hungarian Geological Society, Budapest (Hungary), pp. 394. <https://doi.org/10.1306/M45474>, 1988.
- 1075 Saftić, B., Velić, J., Sztano, O., Juhasz, G., and Ivković, Ž.:~~(2003)~~. Tertiary subsurface facies, source rocks and hydrocarbon reservoirs in the SW part of the Pannonian Basin (Northern Croatia and South-Western Hungary). *Geologia Croatica*, 56/1, 101–122, <https://doi.org/10.4154/232>, 2003.
- 1080 Schmid, S. M., Bernoulli, D., Fügenschuh, B., Matenco, L., Schefer, S., Schuster, R., Tischler, M., and Ustaszewski, K.:~~(2008)~~. The Alpine–Carpathian–Dinaridic orogenic system: correlation and evolution of tectonic units. *Swiss J. Geosci.*, 101, 139–183, <https://doi.org/10.1007/s00015-008-1247-3>, 2008.

- 1085 Schmid, S. M., Fügenschuh, B., Kounov, A., Matenco, L., Nievergelt, P., Oberhänsli, R., Pleuger, J., Schefer, S., Schuster, R., Tomljenović, B., Ustaszewski, K., and Van Hinsbergen, D. J. J.: ~~(2020)~~. Tectonic units of the Alpine collision Zone between Eastern Alps and western Turkey, *Gondwana Research*, **78**, 308-374, <https://doi.org/10.1016/j.gr.2019.07.005>, 2020.
- 1090 Skoko, D., Prelogović, E., and Aljinović, B.: ~~(1987)~~. Geological structure of the Earth's crust above the Moho discontinuity in Yugoslavia, *Geophysical Journal International*, **89**(1), 379–382, <https://doi.org/10.1111/j.1365-246X.1987.tb04434.x>, 1987.
- 1095 Snow, A. D., Whitaker, J., Cochran, M., Van den Bossche, J., Mayo, C., Miara I., de Kloe, J., Karney, C., Couwenberg, B., Lostis, G., Dearing, J., Ouzounoudis, G., Filipe, Jurd, B., Gohlke, C., Hoese, D., Itkin, M., May, R., Heitor, Wiedemann, B. M., Little, B., Barker, C., Willoughby, C., Habertür, D., Popov, E., Holl, G., de Maeyer, J., Ranalli, J., Evers K., and da Costa, M. A.: ~~(2021)~~. pyproj4/pyproj: 3.3.0 Release (3.3.0), *Zenodo*, <https://doi.org/10.5281/zenodo.5709037>, 2021.
- 1100 Środoń, J., Anczkiewicz, A. A., Dunkl, I., Vlahović, I., Velić, I., Tomljenović, B., Kawiak, T., Banaś, M., and Von Eynatten, H.: ~~(2018)~~. Thermal history of the central part of the Karst Dinarides, Croatia: combined application of clay mineralogy and low-T thermochronology, *Tectonophysics*, **744**, 155–176, <https://doi.org/10.1016/j.tecto.2018.06.016>, 2018.
- Stipčević, J., Tkalčić, H., Herak, M., and Markušić, S.: ~~(2011)~~. Crustal and uppermost mantle structure beneath the External Dinarides, Croatia, determined from teleseismic receiver functions, *Geophys. J. Int.*, **185**, pp-1103–1119, doi: 10.1111/j.1365-246X.2011.05004.x, 2011.
- 1105 Stipčević, J., Herak, M., Molinari, I., Dasović, I., Tkalčić, H., and Gosar, A.: ~~(2020)~~. Crustal thickness beneath the Dinarides and surrounding areas from receiver functions, *Tectonics*, **37**, <https://doi.org/10.1029/2019TC005872>, 2020.
- 1110 Šumanovac, F.: ~~(2010)~~. Lithosphere structure at the contact of the Adriatic microplate and the Pannonian segment based on the gravity modelling, *Tectonophysics*, **485/1-4**, 94–106, <https://doi.org/10.1016/j.tecto.2009.12.005>, 2010.
- Šumanovac, F., Orešković, J., Grad, M., and ALP 2002 Working Group: ~~(2009)~~. Crustal structure at the contact of the Dinarides and Pannonian basin based on 2-D seismic and gravity interpretation of the Alp07 profile in the ALP 2002 experiment, *Geophys. J. Int.*, **179**, 615–633, <https://doi.org/10.1111/j.1365-246X.2009.04288.x>, 2009.
- 1115 Šumanovac, F., Hegedűs, E., Orešković, J., Kolar, S., Kovács, A. C., Dudjak, D., and Kovács, I. J.: ~~(2016)~~. Passive seismic experiment and receiver functions analysis to determine crustal

structure at the contact of the northern Dinarides and southwestern Pannonian Basin, *Geophys. J. Int.*, 205, pp-1420–1436, doi: 10.1093/gji/ggw101, 2016.

1120 ~~Tari, V., and Pamić, J. (1998). Geodynamic evolution of the northern Dinarides and the southern part of the Pannonian Basin. *Tectonophysics* 297, 269–281, [https://doi.org/10.1016/S0040-1951\(98\)00172-3](https://doi.org/10.1016/S0040-1951(98)00172-3)~~

1125 Tari, G., Dövényi, P., Dunkl, I., Horváth, F., Lenkey, L., Stefanescu, M., Szafián, P., and Tóth, T.: ~~(1999)~~. Lithosphere structure of the Pannonian basin derived from seismic, gravity and geothermal data, in: ~~Durand, B., Jolivet, L., Horváth, F., and Séranne, M. (Eds.)~~ The Mediterranean Basins: Tertiary Extension within the Alpine Orogen, ~~edited by Durand, B., Jolivet, L., Horváth, F., and Séranne, M.~~, Geological Society of London, Special Publications, 156, 215–250, <https://doi.org/10.1144/GSL.SP.1999.156.01.12>, 1999.

1130 Tišljarić, J., Vlahović, I., Velić, I., and Sokač, B.: ~~(2002)~~. Carbonate platform megafacies of the Jurassic and Cretaceous deposits of the Karst Dinarides, *Geologia Croatica*, 55/2, 139–170, [2002](https://doi.org/10.1144/GSL.SP.1999.156.01.12).

Tozer, B., Sandwell, D.T., Smith, W. H. F., Olson, C., Beale, J. R., and Wessel, P.: ~~(2019)~~. Global bathymetry and topography at 15 arc sec: SRTM15+, *Earth and Space Science*, 6, 1847–1864, <https://doi.org/10.1029/2019EA000658>, 2019.

1135 Ustaszewski, K., Schmid, S. M., Fügenschuh, B., Tischler, M., Kissling, E., and Spakman, W.: ~~(2008)~~. A map-view restoration of the Alpine–Carpathian–Dinaridic system for Early Miocene, *Swiss Journal of Geosciences*, 101, Supplement 1, 273–294, <https://doi.org/10.1007/s00015-008-1288-7><https://doi.org/10.1007/s00015-008-1288-7>, 2008.

1140 Ustaszewski, K., Schmid, S. M., Lugović, B., Schuster, R., Schlatter, U., Bernoulli, D., Hottinger, L., Kounov, A., Fügenschuh, B., and Schefer, S.: ~~(2009)~~. Late Cretaceous intra-oceanic magmatism in the internal Dinarides (northern Bosnia and Herzegovina): Implication for the collision of the Adriatic and European Plates, *Lithos*, 108, 106–125, <https://doi.org/10.1016/j.lithos.2008.09.010><https://doi.org/10.1016/j.lithos.2008.09.010>, 2009.

1145 [Velić, I., Vlahović, I., and Matičec, D.: \*Depositional sequences and palaeogeography of the Adriatic Carbonate Platform\*, \*Mem. Soc. Geol. Ital.\*, 57, 141–151, 2002.](https://doi.org/10.1016/j.lithos.2008.09.010)

Vlahović, I., Tišljarić, J., Velić, I., and Matičec, D.: ~~(2005)~~. Evolution of the Adriatic Carbonate Platform: Palaeogeography, main events and depositional dynamics. *Palaeogeogr. Palaeoclimatol. Palaeoecol.*, 220/3–4, 333–360.

1150 <https://doi.org/10.1016/j.palaeo.2005.01.011><https://doi.org/10.1016/j.palaeo.2005.01.011>  
 11, 2005.

## Appendix A

1155 **Table A1.** Estimation of Carbonate Rock Complex (CRC) bottom depth in Dinarides. CRC bottom  
 depths were estimated based on 93 sheets of Basic Geological Map (1:100,000) of former Yugoslavia  
 (Osnovna Geološka Karta SFRJ) and 1:200,000 Geological Map of Albania (Geological Map of Albania,  
 2002). The CRC bottom depth values were estimated for each map centroid, in respect to External  
 1160 Dinarides structural relations, deformation styles that incorporate thrusting, folding (e.g. Balling et  
 al., 2021), and thicknesses of deposits on individual maps. Regional nappe systems in External  
 Dinarides incorporate up to six individual structural levels composed of thrust sheets of laterally  
 and/or vertically variable thicknesses, enabling estimated combined absolute CRC depth up to  
 14,200 m.

No.	Basic Geological Map (BGM)	BGM centroid coordinates		Estimated average elevation (m a.s.l.)	Estimated absolute bedrock depth (m)	Number of structural levels
		Latitude ( $\varphi$ )	Longitude ( $\lambda$ )			
1	Albania Nord	<a href="#">42.090</a>	<a href="#">20.048</a>	<a href="#">805</a>	<a href="#">8200-14200</a>	<a href="#">2-5</a>
2	Banja Luka	<a href="#">44.834</a>	<a href="#">17.247</a>	<a href="#">300</a>	<a href="#">1200</a>	<a href="#">0-2</a>
3	Bar	<a href="#">42.167</a>	<a href="#">19.243</a>	<a href="#">400</a>	<a href="#">11100</a>	<a href="#">2-4</a>
4	Bihać	<a href="#">44.836</a>	<a href="#">15.742</a>	<a href="#">600</a>	<a href="#">8400</a>	<a href="#">2-3</a>
5	Bijeljina	<a href="#">44.831</a>	<a href="#">19.245</a>	=	Saftić et al. (2003)	=
6	Biograd	<a href="#">43.830</a>	<a href="#">15.244</a>	<a href="#">-40</a>	<a href="#">7900</a>	<a href="#">1-2</a>
7	Biševo	<a href="#">42.833</a>	<a href="#">16.243</a>	<a href="#">-70</a>	<a href="#">7600</a>	<a href="#">1-2</a>

<u>8</u>	<u>Bosanska Krupa</u>	<u>44.832</u>	<u>16.247</u>	<u>400</u>	<u>3700</u>	<u>0-2</u>
<u>9</u>	<u>Bosanski Novi</u>	<u>45.165</u>	<u>16.242</u>	<u>200</u>	<u>200</u>	<u>0</u>
<u>10</u>	<u>Brčko</u>	<u>44.831</u>	<u>18.739</u>	<u>=</u>	<u>Saftić et al. (2003)</u>	<u>=</u>
<u>11</u>	<u>Budva</u>	<u>42.167</u>	<u>18.747</u>	<u>-100</u>	<u>9100</u>	<u>2-4</u>
<u>12</u>	<u>Bugojno</u>	<u>44.160</u>	<u>17.233</u>	<u>900</u>	<u>6500</u>	<u>1-3</u>
<u>13</u>	<u>Cres</u>	<u>44.836</u>	<u>14.249</u>	<u>0</u>	<u>7200</u>	<u>1-2</u>
<u>14</u>	<u>Crikvenica</u>	<u>45.171</u>	<u>14.741</u>	<u>400</u>	<u>8300</u>	<u>2-3</u>
<u>15</u>	<u>Črnomelj</u>	<u>45.504</u>	<u>15.251</u>	<u>350</u>	<u>8200</u>	<u>1-2</u>
<u>16</u>	<u>Delnice</u>	<u>45.504</u>	<u>14.739</u>	<u>600</u>	<u>7900</u>	<u>1-2</u>
<u>17</u>	<u>Derventa</u>	<u>44.832</u>	<u>17.740</u>	<u>250</u>	<u>200</u>	<u>0-1</u>
<u>18</u>	<u>Doboj</u>	<u>44.837</u>	<u>18.246</u>	<u>=</u>	<u>Saftić et al. (2003)</u>	<u>=</u>
<u>19</u>	<u>Drniš</u>	<u>43.832</u>	<u>16.251</u>	<u>500</u>	<u>9000</u>	<u>2-3</u>
<u>20</u>	<u>Drvar</u>	<u>44.499</u>	<u>16.240</u>	<u>700</u>	<u>7800</u>	<u>2-3</u>
<u>21</u>	<u>Dubrovnik</u>	<u>42.497</u>	<u>18.244</u>	<u>200</u>	<u>9000</u>	<u>2-3</u>
<u>22</u>	<u>Foča</u>	<u>43.499</u>	<u>18.754</u>	<u>1000</u>	<u>300</u>	<u>0-1</u>
<u>23</u>	<u>Gacko</u>	<u>43.166</u>	<u>18.746</u>	<u>1300</u>	<u>10400</u>	<u>1-5</u>
<u>24</u>	<u>Glamoč</u>	<u>44.168</u>	<u>16.746</u>	<u>1000</u>	<u>8500</u>	<u>2-3</u>



<a href="#">25</a>	<a href="#">Gorica</a>	<a href="#">45.830</a>	<a href="#">13.747</a>	<a href="#">350</a>	<a href="#">7400</a>	<a href="#">2-3</a>
<a href="#">26</a>	<a href="#">Gospić</a>	<a href="#">44.496</a>	<a href="#">15.247</a>	<a href="#">500</a>	<a href="#">10400</a>	<a href="#">3-4</a>
<a href="#">27</a>	<a href="#">Ilirska Bistrica</a>	<a href="#">45.502</a>	<a href="#">14.240</a>	<a href="#">400</a>	<a href="#">7900</a>	<a href="#">2-3</a>
<a href="#">28</a>	<a href="#">Imotski</a>	<a href="#">43.502</a>	<a href="#">17.246</a>	<a href="#">800</a>	<a href="#">13000</a>	<a href="#">2-4</a>
<a href="#">29</a>	<a href="#">Jabuka</a>	<a href="#">43.164</a>	<a href="#">15.266</a>	<a href="#">-150</a>	<a href="#">7700</a>	<a href="#">1-2</a>
<a href="#">30</a>	<a href="#">Jajce</a>	<a href="#">44.492</a>	<a href="#">17.246</a>	<a href="#">600</a>	<a href="#">4100</a>	<a href="#">1-3</a>
<a href="#">31</a>	<a href="#">Jelsa</a>	<a href="#">43.169</a>	<a href="#">16.742</a>	<a href="#">0</a>	<a href="#">8900</a>	<a href="#">1-2</a>
<a href="#">32</a>	<a href="#">Kalinovik</a>	<a href="#">43.496</a>	<a href="#">18.247</a>	<a href="#">900</a>	<a href="#">9000</a>	<a href="#">1-4</a>
<a href="#">33</a>	<a href="#">Karlovac</a>	<a href="#">45.502</a>	<a href="#">15.750</a>	<a href="#">200</a>	<a href="#">1000</a>	<a href="#">0-2</a>
<a href="#">34</a>	<a href="#">Ključ</a>	<a href="#">44.501</a>	<a href="#">16.743</a>	<a href="#">700</a>	<a href="#">7500</a>	<a href="#">2-3</a>
<a href="#">35</a>	<a href="#">Knin</a>	<a href="#">44.166</a>	<a href="#">16.246</a>	<a href="#">550</a>	<a href="#">9500</a>	<a href="#">2-3</a>
<a href="#">36</a>	<a href="#">Korčula</a>	<a href="#">42.836</a>	<a href="#">17.246</a>	<a href="#">-50</a>	<a href="#">6600</a>	<a href="#">1-2</a>
<a href="#">37</a>	<a href="#">Kostajnica</a>	<a href="#">45.167</a>	<a href="#">16.751</a>	<a href="#">250</a>	<a href="#">200</a>	<a href="#">0</a>
<a href="#">38</a>	<a href="#">Kotor</a>	<a href="#">42.500</a>	<a href="#">18.743</a>	<a href="#">700</a>	<a href="#">10300</a>	<a href="#">2-5</a>
<a href="#">39</a>	<a href="#">Kranj</a>	<a href="#">46.158</a>	<a href="#">14.141</a>	<a href="#">700</a>	<a href="#">6800.00</a>	<a href="#">2-3</a>
<a href="#">40</a>	<a href="#">Labin</a>	<a href="#">45.169</a>	<a href="#">14.245</a>	<a href="#">300</a>	<a href="#">6500</a>	<a href="#">1-2</a>
<a href="#">41</a>	<a href="#">Lastovo</a>	<a href="#">42.836</a>	<a href="#">16.745</a>	<a href="#">-80</a>	<a href="#">8100</a>	<a href="#">1-2</a>

<a href="#">42</a>	<a href="#">Livno</a>	<a href="#">43.835</a>	<a href="#">17.246</a>	<a href="#">1100</a>	<a href="#">11200</a>	<a href="#">2-4</a>
<a href="#">43</a>	<a href="#">Lošinj</a>	<a href="#">44.503</a>	<a href="#">14.241</a>	<a href="#">0</a>	<a href="#">6200</a>	<a href="#">1-2</a>
<a href="#">44</a>	<a href="#">Ljubovija</a>	<a href="#">44.147</a>	<a href="#">19.245</a>	<a href="#">500</a>	<a href="#">100</a>	<a href="#">0-1</a>
<a href="#">45</a>	<a href="#">Metković</a>	<a href="#">43.167</a>	<a href="#">17.750</a>	<a href="#">250</a>	<a href="#">13100</a>	<a href="#">3-4</a>
<a href="#">46</a>	<a href="#">Molat</a>	<a href="#">44.163</a>	<a href="#">14.745</a>	<a href="#">-50</a>	<a href="#">7200</a>	<a href="#">1-2</a>
<a href="#">47</a>	<a href="#">Mostar</a>	<a href="#">43.500</a>	<a href="#">17.740</a>	<a href="#">900</a>	<a href="#">13500</a>	<a href="#">4-5</a>
<a href="#">48</a>	<a href="#">Nevesinje</a>	<a href="#">43.163</a>	<a href="#">18.242</a>	<a href="#">1000</a>	<a href="#">14100</a>	<a href="#">4-5</a>
<a href="#">49</a>	<a href="#">Nikšić</a>	<a href="#">42.833</a>	<a href="#">18.750</a>	<a href="#">1000</a>	<a href="#">12600</a>	<a href="#">5-6</a>
<a href="#">50</a>	<a href="#">Nova Gradiška</a>	<a href="#">45.167</a>	<a href="#">17.247</a>	<a href="#">=</a>	<a href="#">Saftić et al. (2003)</a>	<a href="#">=</a>
<a href="#">51</a>	<a href="#">Nova Kapela</a>	<a href="#">45.165</a>	<a href="#">17.743</a>	<a href="#">=</a>	<a href="#">Saftić et al. (2003)</a>	<a href="#">=</a>
<a href="#">52</a>	<a href="#">Novo Mesto</a>	<a href="#">45.837</a>	<a href="#">15.240</a>	<a href="#">250</a>	<a href="#">7300</a>	<a href="#">1-2</a>
<a href="#">53</a>	<a href="#">Obrovac</a>	<a href="#">44.170</a>	<a href="#">15.746</a>	<a href="#">300</a>	<a href="#">10000</a>	<a href="#">2-3</a>
<a href="#">54</a>	<a href="#">Ogulin</a>	<a href="#">45.171</a>	<a href="#">15.250</a>	<a href="#">400</a>	<a href="#">9400</a>	<a href="#">2-3</a>
<a href="#">55</a>	<a href="#">Omiš</a>	<a href="#">43.502</a>	<a href="#">16.751</a>	<a href="#">450</a>	<a href="#">10200</a>	<a href="#">2-4</a>
<a href="#">56</a>	<a href="#">Otočac</a>	<a href="#">44.829</a>	<a href="#">15.248</a>	<a href="#">500</a>	<a href="#">10200</a>	<a href="#">3-4</a>
<a href="#">57</a>	<a href="#">Ploče</a>	<a href="#">43.169</a>	<a href="#">17.246</a>	<a href="#">250</a>	<a href="#">10500</a>	<a href="#">2-4</a>
<a href="#">58</a>	<a href="#">Pljevlja</a>	<a href="#">43.490</a>	<a href="#">19.261</a>	<a href="#">1000</a>	<a href="#">200</a>	<a href="#">0-1</a>

<a href="#">59</a>	<a href="#">Postojna</a>	<a href="#">45.835</a>	<a href="#">14.249</a>	<a href="#">700</a>	<a href="#">7700.00</a>	<a href="#">2-3</a>
<a href="#">60</a>	<a href="#">Prača</a>	<a href="#">43.814</a>	<a href="#">18.749</a>	<a href="#">1000</a>	<a href="#">0</a>	<a href="#">0-1</a>
<a href="#">61</a>	<a href="#">Prijedor</a>	<a href="#">44.834</a>	<a href="#">16.741</a>	<a href="#">400</a>	<a href="#">2400</a>	<a href="#">0-2</a>
<a href="#">62</a>	<a href="#">Primošten</a>	<a href="#">43.504</a>	<a href="#">15.750</a>	<a href="#">-100</a>	<a href="#">7600</a>	<a href="#">1-2</a>
<a href="#">63</a>	<a href="#">Prozor</a>	<a href="#">43.824</a>	<a href="#">17.743</a>	<a href="#">1100</a>	<a href="#">7500</a>	<a href="#">0-4</a>
<a href="#">64</a>	<a href="#">Pula</a>	<a href="#">44.831</a>	<a href="#">13.743</a>	<a href="#">0</a>	<a href="#">4600</a>	<a href="#">1</a>
<a href="#">65</a>	<a href="#">Rab</a>	<a href="#">44.829</a>	<a href="#">14.742</a>	<a href="#">100</a>	<a href="#">9200</a>	<a href="#">2-3</a>
<a href="#">66</a>	<a href="#">Ribnica</a>	<a href="#">45.837</a>	<a href="#">14.751</a>	<a href="#">600</a>	<a href="#">7200</a>	<a href="#">1-2</a>
<a href="#">67</a>	<a href="#">Rovinj</a>	<a href="#">45.165</a>	<a href="#">13.749</a>	<a href="#">20</a>	<a href="#">4500</a>	<a href="#">1</a>
<a href="#">68</a>	<a href="#">Sarajevo</a>	<a href="#">43.829</a>	<a href="#">18.253</a>	<a href="#">700</a>	<a href="#">2600</a>	<a href="#">1-3</a>
<a href="#">69</a>	<a href="#">Šavnik</a>	<a href="#">42.833</a>	<a href="#">19.252</a>	<a href="#">1000</a>	<a href="#">10600</a>	<a href="#">1-5</a>
<a href="#">70</a>	<a href="#">Šibenik</a>	<a href="#">43.837</a>	<a href="#">15.741</a>	<a href="#">50</a>	<a href="#">8000</a>	<a href="#">2-3</a>
<a href="#">71</a>	<a href="#">Silba</a>	<a href="#">44.496</a>	<a href="#">14.744</a>	<a href="#">0</a>	<a href="#">8000</a>	<a href="#">2-3</a>
<a href="#">72</a>	<a href="#">Sinj</a>	<a href="#">43.835</a>	<a href="#">16.749</a>	<a href="#">800</a>	<a href="#">12000</a>	<a href="#">3-4</a>
<a href="#">73</a>	<a href="#">Slavonski Brod</a>	<a href="#">45.170</a>	<a href="#">18.239</a>	<a href="#">=</a>	<a href="#">Saftić et al. (2003)</a>	<a href="#">=</a>
<a href="#">74</a>	<a href="#">Slunj</a>	<a href="#">45.169</a>	<a href="#">15.746</a>	<a href="#">350</a>	<a href="#">4500</a>	<a href="#">0-2</a>
<a href="#">75</a>	<a href="#">Split</a>	<a href="#">43.500</a>	<a href="#">16.244</a>	<a href="#">100</a>	<a href="#">7500</a>	<a href="#">1-2</a>

<a href="#">76</a>	<a href="#">Ston</a>	<a href="#">42.834</a>	<a href="#">17.748</a>	<a href="#">200</a>	<a href="#">9000</a>	<a href="#">1-3</a>
<a href="#">77</a>	<a href="#">Svetac</a>	<a href="#">43.171</a>	<a href="#">15.746</a>	<a href="#">-150</a>	<a href="#">7700</a>	<a href="#">1-2</a>
<a href="#">78</a>	<a href="#">Teslić</a>	<a href="#">44.491</a>	<a href="#">17.736</a>	<a href="#">700</a>	<a href="#">700</a>	<a href="#">0-3</a>
<a href="#">79</a>	<a href="#">Titograd</a>	<a href="#">42.500</a>	<a href="#">19.253</a>	<a href="#">700</a>	<a href="#">12200</a>	<a href="#">4-5</a>
<a href="#">80</a>	<a href="#">Tolmin</a>	<a href="#">46.153</a>	<a href="#">13.610</a>	<a href="#">700</a>	<a href="#">6600.00</a>	<a href="#">2-3</a>
<a href="#">81</a>	<a href="#">Trebinje</a>	<a href="#">42.830</a>	<a href="#">18.249</a>	<a href="#">700</a>	<a href="#">12000</a>	<a href="#">2-4</a>
<a href="#">82</a>	<a href="#">Trst</a>	<a href="#">45.497</a>	<a href="#">13.741</a>	<a href="#">200</a>	<a href="#">6000</a>	<a href="#">2-3</a>
<a href="#">83</a>	<a href="#">Tuzla</a>	<a href="#">44.489</a>	<a href="#">18.742</a>	<a href="#">400</a>	<a href="#">300</a>	<a href="#">0-1</a>
<a href="#">84</a>	<a href="#">Udbina</a>	<a href="#">44.503</a>	<a href="#">15.750</a>	<a href="#">800</a>	<a href="#">12000</a>	<a href="#">3-4</a>
<a href="#">85</a>	<a href="#">Ulcinj</a>	<a href="#">41.825</a>	<a href="#">19.244</a>	<a href="#">-200</a>	<a href="#">9200</a>	<a href="#">2-3</a>
<a href="#">86</a>	<a href="#">Vareš</a>	<a href="#">44.144</a>	<a href="#">18.245</a>	<a href="#">800</a>	<a href="#">1600</a>	<a href="#">0-1</a>
<a href="#">87</a>	<a href="#">Vis</a>	<a href="#">43.166</a>	<a href="#">16.250</a>	<a href="#">-70</a>	<a href="#">7600</a>	<a href="#">1-2</a>
<a href="#">88</a>	<a href="#">Višegrad</a>	<a href="#">43.813</a>	<a href="#">19.271</a>	<a href="#">700</a>	<a href="#">700</a>	<a href="#">0-1</a>
<a href="#">89</a>	<a href="#">Vlasenica</a>	<a href="#">44.147</a>	<a href="#">18.745</a>	<a href="#">600</a>	<a href="#">700</a>	<a href="#">0-1</a>
<a href="#">90</a>	<a href="#">Žabljak</a>	<a href="#">43.166</a>	<a href="#">19.250</a>	<a href="#">1200</a>	<a href="#">2400</a>	<a href="#">1-5</a>
<a href="#">91</a>	<a href="#">Zadar</a>	<a href="#">44.163</a>	<a href="#">15.245</a>	<a href="#">10</a>	<a href="#">8000</a>	<a href="#">2-3</a>
<a href="#">92</a>	<a href="#">Zavidovići</a>	<a href="#">44.495</a>	<a href="#">18.252</a>	<a href="#">350</a>	<a href="#">0</a>	<a href="#">0</a>
<a href="#">93</a>	<a href="#">Zenica</a>	<a href="#">44.149</a>	<a href="#">17.733</a>	<a href="#">800</a>	<a href="#">1200</a>	<a href="#">0-3</a>

<u>94</u>	<u>Zvornik</u>	<u>44.489</u>	<u>19.245</u>	<u>250</u>	<u>800</u>	<u>0-1</u>
-----------	----------------	---------------	---------------	------------	------------	------------

## Appendix B

### Point locations of data used

The following figure shows the exact location of data points used for interpolation of model interfaces and parameters. Data points used for each interface and parameter are shown in a separate figure panel.

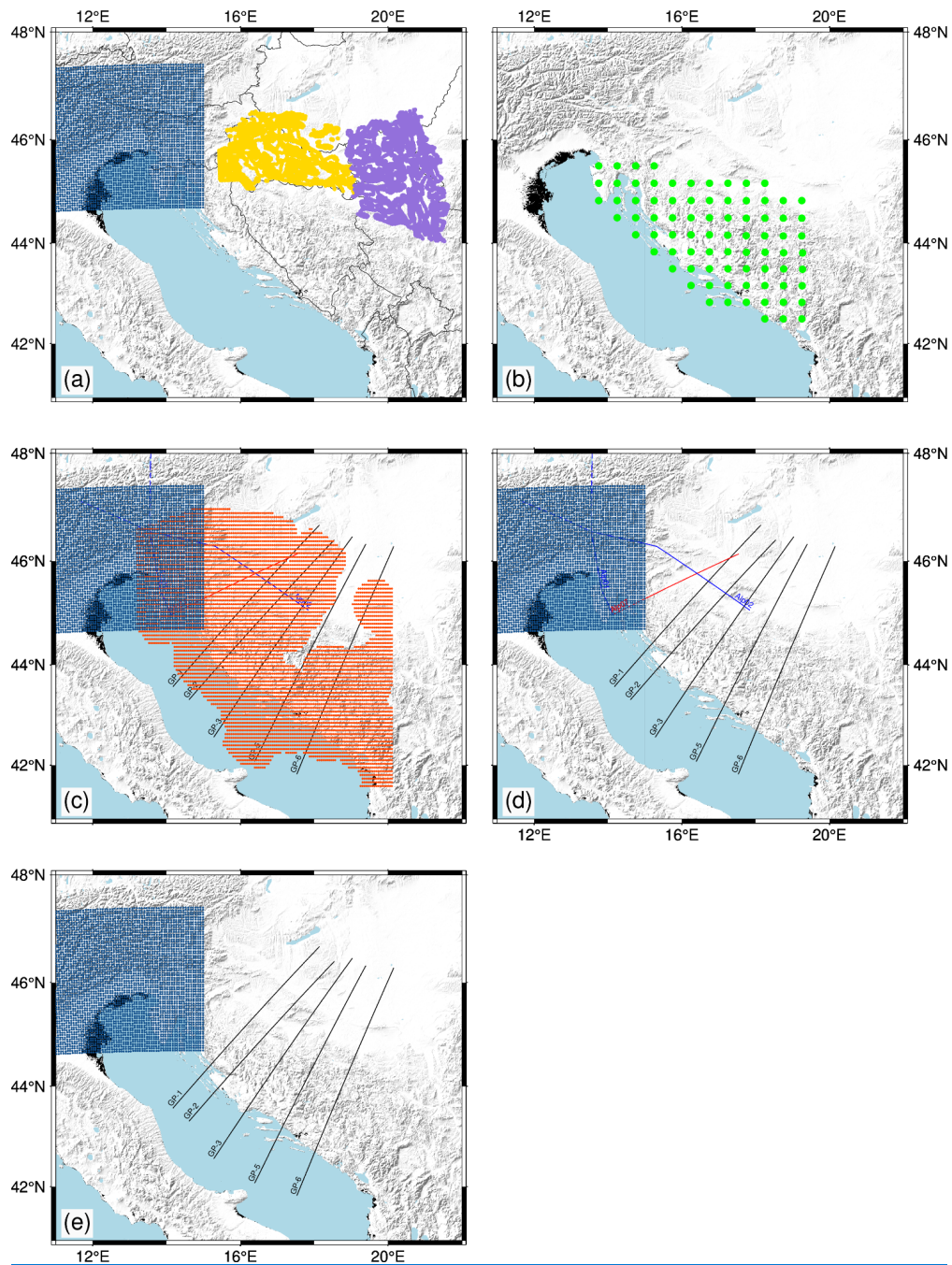




Fig. B1 Point locations of data used for interpolation of (a) sediment bottom depth, (b) CRC depth, (c) Moho depth, (d) P-wave velocity, (e) density. Yellow points mark data from Saftić et al. (2003), purple points mark data from Matenco & Radivojević (2012), green points mark data on CRC depths, blue points mark data from the NAC model (Magrin & Rossi, 2020), orange points mark data from Stipčević et al. (2011), blue lines mark the positions of profiles from Brückl et al. (2007), red lines mark the profile from Šumanovac et al. (2009), and black lines mark the gravimetric profiles from Šumanovac (2010).

## 1180 Appendix CA

### Kriging

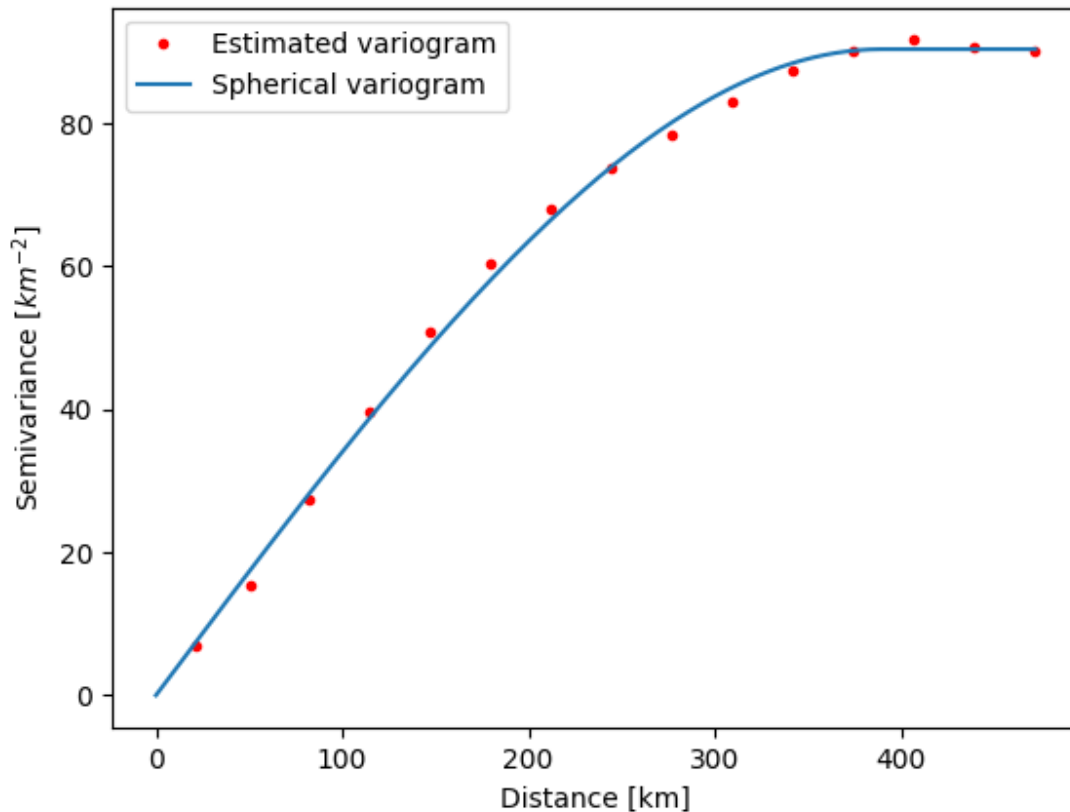
1185 Kriging is a method of interpolation formulated for the estimation of a continuous spatial attribute (e.g. depth to Moho interface) at an unknown site, using the limited set of data from sampled sites. It is a form of generalized linear regression used for the formulation of an optimal estimator in a minimum mean square error sense (Olea, 1999).

Generally, the value at a point of interest is calculated as follows:

$$\hat{Z}(x_0) = \sum_{i=1}^n \lambda_i Z(x_i),$$

where  $\hat{Z}(x_0)$  is value estimation at point of interest  $x_0$ ,  $\lambda_i$  are weights, and  $Z(x_i)$  are known values at sites  $x_i$ . The kriging weights are derived from the covariance of the sampled values.

1190 The first step in kriging interpolation is estimation of the variogram (also called a semivariogram) – a statistic that assesses the average decrease in similarity between two random variables as the distance between them increases. It is the inverse of covariance – the covariance measures similarity, and the variogram measures dissimilarity. Unlike the other moments (e.g. the mean), the variogram is not a single number, but a continuous  
1195 function of a variable  $h$ , called the lag. The variogram calculated from the sampled points is called the experimental variogram. The experimental variogram is not used in the calculation of kriging weights but is used to fit a theoretical variogram which in turn is used for calculation of the weights. When fitting, we can use limited types of semivariograms which have acceptable properties needed for solving the system of equations in order to obtain the  
1200 weights. If we would use the experimental variogram directly, we might end up with an unsolvable system of equations. For example, **Fig. CA1** shows an experimental and theoretical variogram used for interpolation of Moho interface depth. A variogram, such as the one in **Fig. CA1**, that increases in dissimilarity with distance over short lags and then levels off is called a transitive variogram. The lag at which it reaches a constant value is called  
1205 the range, and that constant value is called the sill. For the Moho depth interpolation, we had an abundance of data available, and we were able to estimate a theoretical variogram which fits the observed data almost perfectly.



1210 | **Fig. CA1.** Estimated and theoretical (spherical) variogram used for interpolation of Moho interface depth.

1215 | In case of other model parameters, we did not have such a perfect fit for larger lags. For instance, **Fig. CA2** shows the variogram used for Neogene deposits bottom interpolation. In this case, the theoretical variogram was not spherical, but exponential. In this case, for the largest lags shown, the theoretical and estimated variograms do not fit. For the calculation of the variogram pairs of measured values are used. Since for the greater distances (greater lags) there are fewer numbers of such pairs, the estimates are less accurate for those lags. Fortunately, for practical use in kriging, the variogram closer to the origin requires the most accurate estimation (Olea, 1999), and we had that condition met for all our model

1220 | parameters.

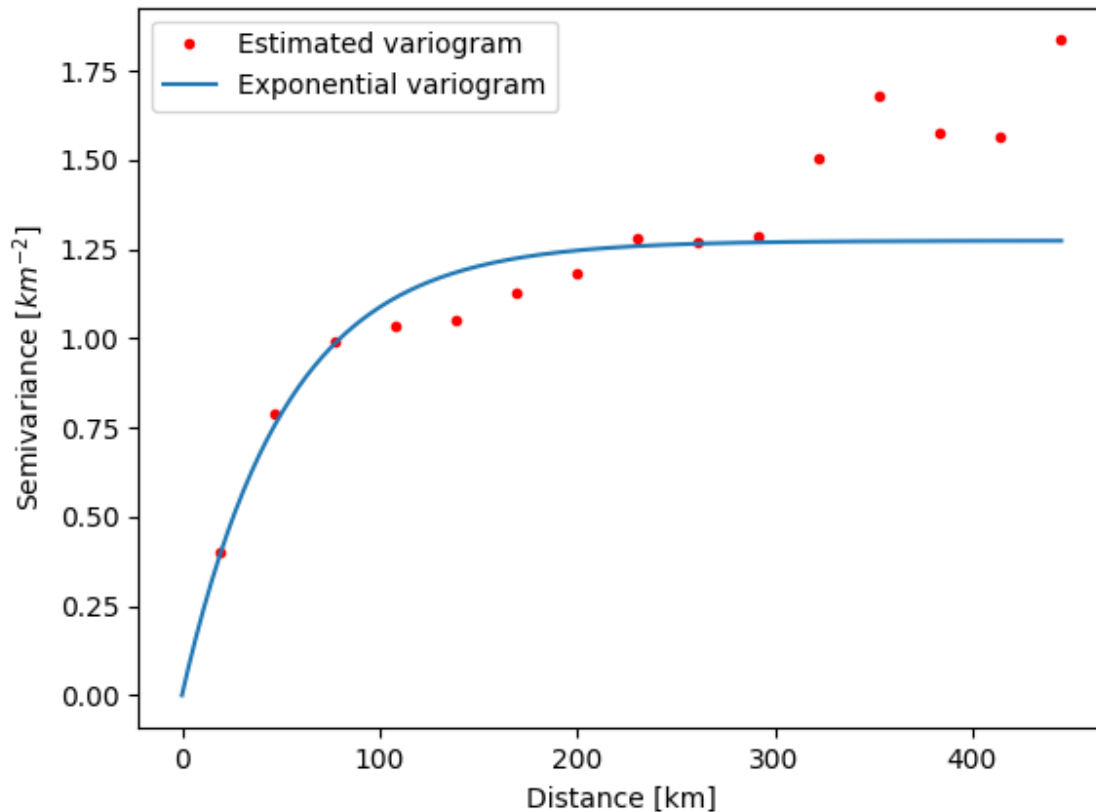
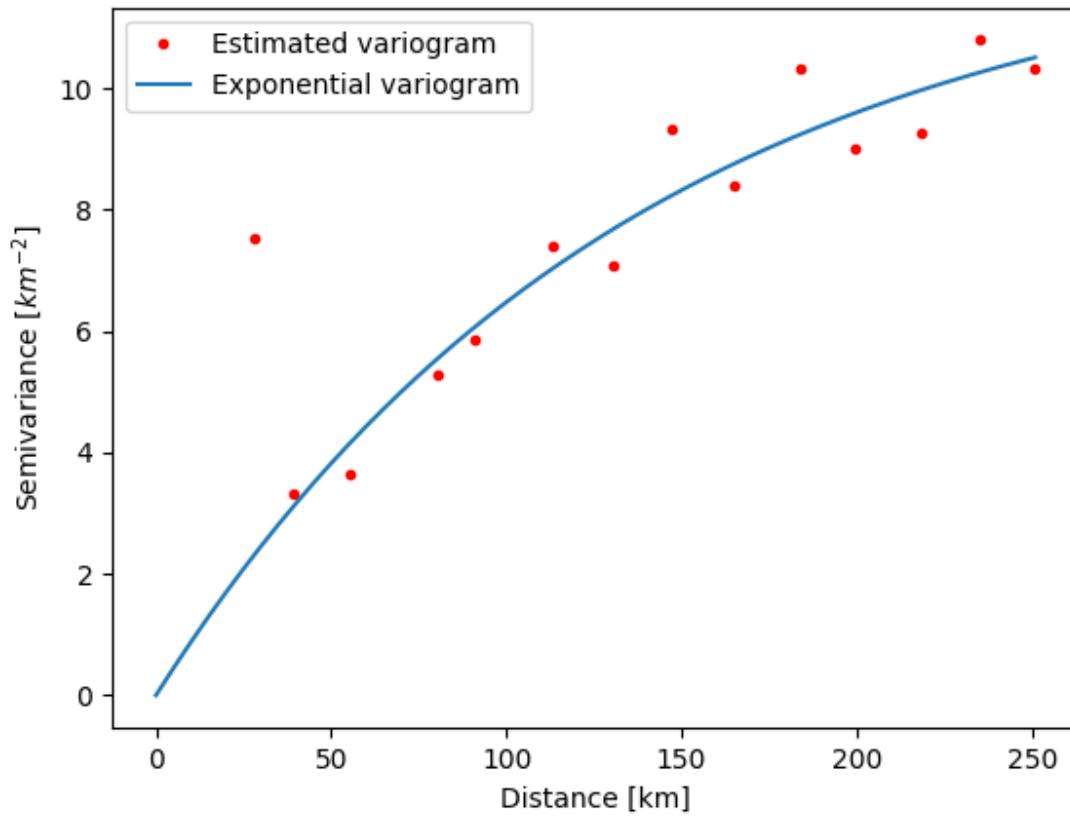


Fig. CA2. Neogene deposits bottom estimated and theoretical (exponential) variograms.

1225

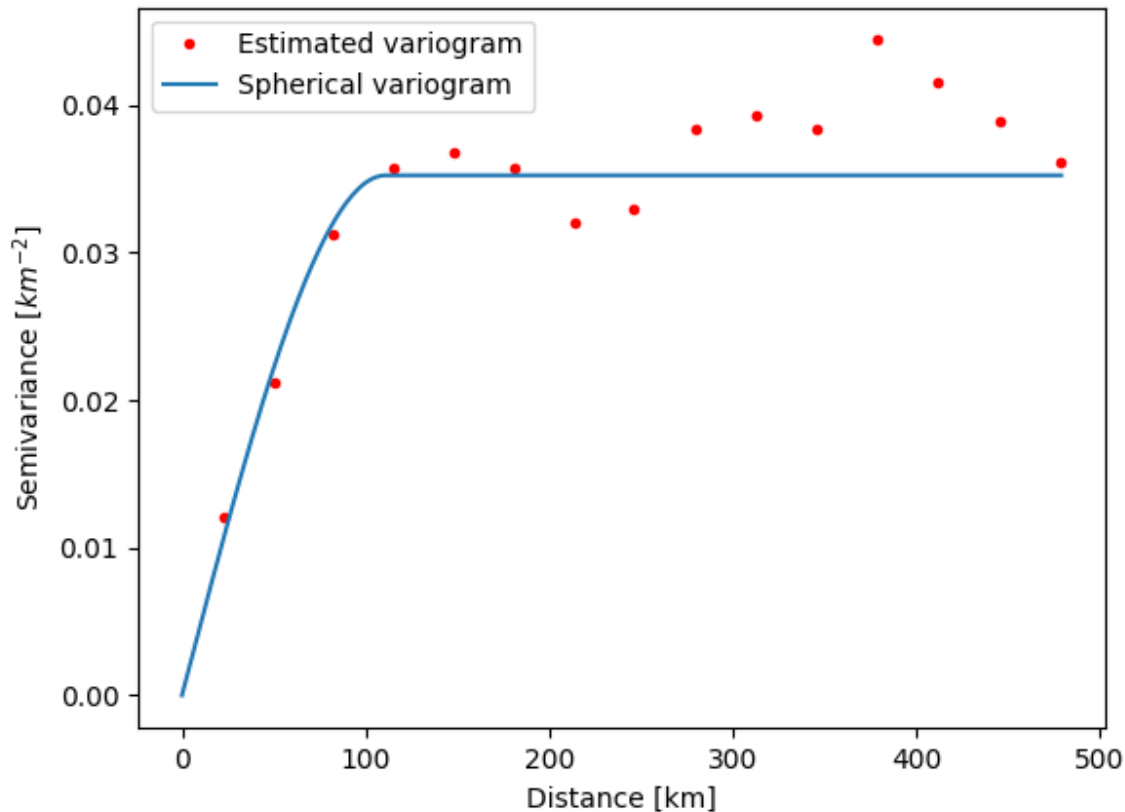
Variograms for [CRC Carbonate complex](#) bottom depth and velocity estimation are shown in **Figs. CA3** and **CA4**, respectively. Crust velocity variogram shown in **Fig. CA4**. is required to have a constant mean in the sample space in order to be able to estimate a variogram. In case of a gentle and systematic variation in the mean (called the drift), e.g. velocity increases with depth, it has to be removed prior to the estimation of the variogram. Such a drift was indeed observed, and was removed prior to the estimation of the variogram shown in **Fig. CA4**. Besides the drift, we estimated the experimental variogram in several directions, in order to check if it was dependent on the direction (i.e. if there was anisotropy), but we have not observed any anisotropy.

1230



1235

**Fig CA3.** Carbonate [Rock Complex \(CRC\) complex](#) bottom estimated and theoretical (exponential) variogram.



1240 | **Fig. CA4.** Estimated and theoretical (spherical) variogram used for interpolation of the crustal velocity ( $V_p$ ).

1245 | Once we had variograms estimated, we were able to obtain the weights and calculate the values of parameters (Moho, Neogene deposits bottom, [CRC Carbonate complex](#) bottom, velocity) for each point in our grid. All of the operations, both variogram estimation and the interpolation itself, were done using the gstat package (Pebesma, 2004). Alongside the interpolated values, the package also returns the variance estimates for each point in the grid.

1250 | The interface parameters (Moho, Neogene deposits bottom and [CRC Carbonate complex](#) bottom depth) were interpolated using ordinary kriging. Ordinary kriging assumes that the mean of the value is unknown, but constant. For interpolation of the velocity, we had to use a more general type of kriging – the universal kriging. It relaxes the condition on the mean – it is no longer assumed constant. The other properties of kriging are shared between both types used. They are both minimum square error estimates. The estimation is not limited to the data interval (it is possible to extrapolate – although it is less accurate). They have, so  
 1255 | called, declustering ability – the measurements that are spatially clustered have lower weights than isolated points. They are exact interpolators with zero kriging variance –



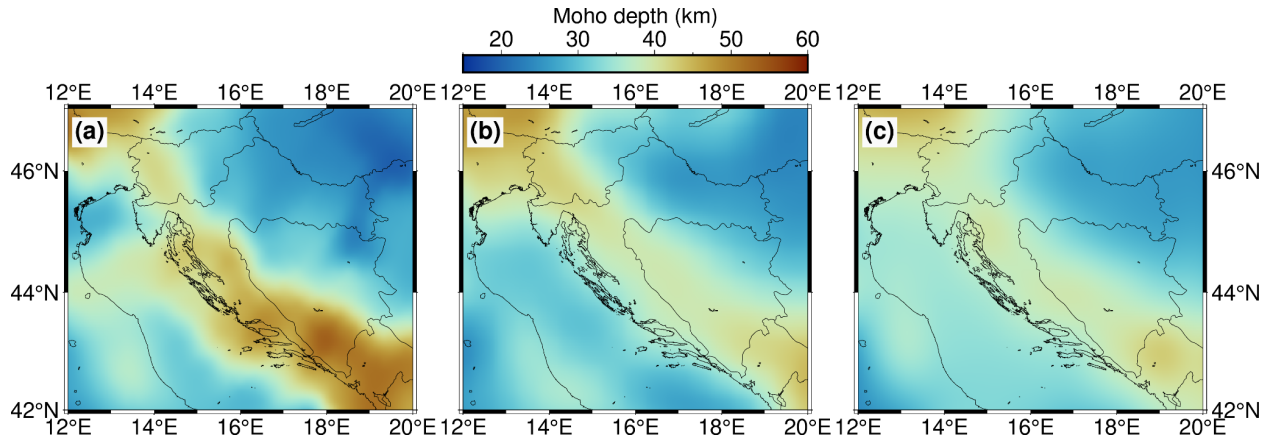
meaning that if, for instance, we try to calculate the value exactly at a sampled point, kriging will return the exact value and assign 0 variance to it. It can be nicely seen in **Fig. 5** showing the velocity variances. Since the variance at sampled sites is zero it is possible to discern the profiles that were sampled for data. Kriging is not able to handle duplicate points – it causes the insolvable systems of equations for the kriging weights – therefore we had to handle such points. It is also worth mentioning that the variance returned by the kriging software does not depend on variance or values of individual observations, but only on the sampling pattern. Therefore, we added the (estimated or available) data variance to the variance obtained from the kriging and called it the total variance.

1260

1265

## Appendix D

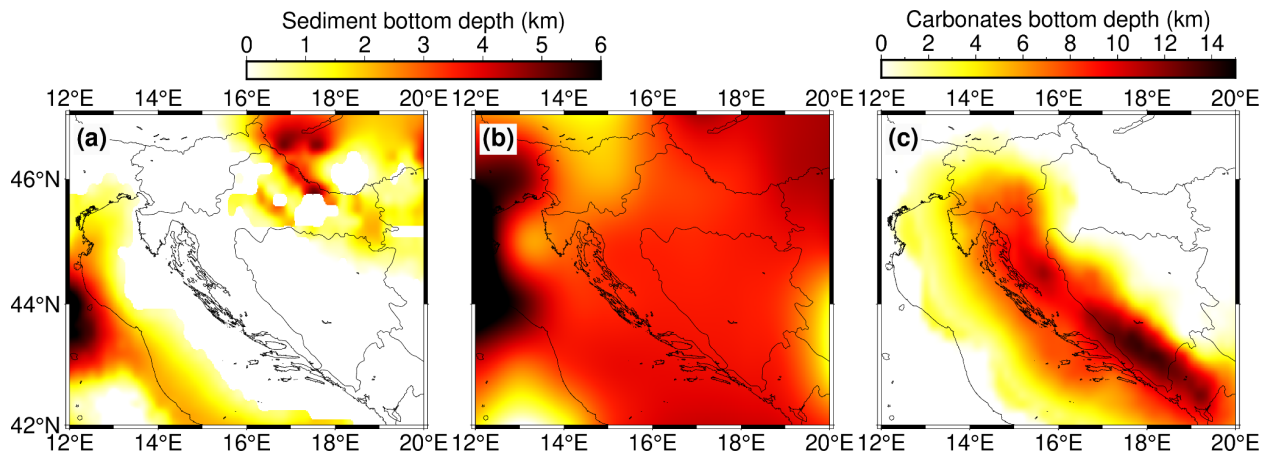
### Comparison of the new model to existing regional models



1270 **Fig. D1** Comparison of Moho depths among (a) our newly derived model, (b) Grad et al. (2009) european Moho model, and (c) EPcrust model (Molinari and Morelli, 2011).

1275 Compared to existing regional models, Moho depth is considerably greater in the new model, especially in the southern part of the Dinarides.

The EPcrust model has sediment bottom depth defined. In our model, we discern CRC bottom and Neogene sediment bottom, which is not defined separately in the (regional) EPcrust model. Therefore we put both of them in Fig. D2.



1280 **Fig. D2** Comparison of sediment bottom depth as defined as (a) Neogene sediment bottom depth in our model, (b) sediment bottom in EPcrust model, and (c) CRC bottom depth in our model.

The horizontal variations in sediment and CRC bottom depths are much more pronounced than in the regional EPcrust model.

1285 [In the EPcrust model, the velocity is defined as two layers \(upper and lower crust\) with](#)  
1290 [constant velocity value \(for a given grid point, it does not vary with depth; it varies](#)  
[horizontally, though\). Therefore, we have picked two depths in our model, since we defined](#)  
[velocity as varying in all three dimensions. Even though we do not define crust as two layers](#)  
[\(lower or upper crust\), we have picked velocity at depth of 15 km to compare with EPcrust](#)  
[upper crust, and velocity at depth of 25 km to compare with EPcrust lower crust. The](#)  
[comparison is shown in Fig. D3.](#)

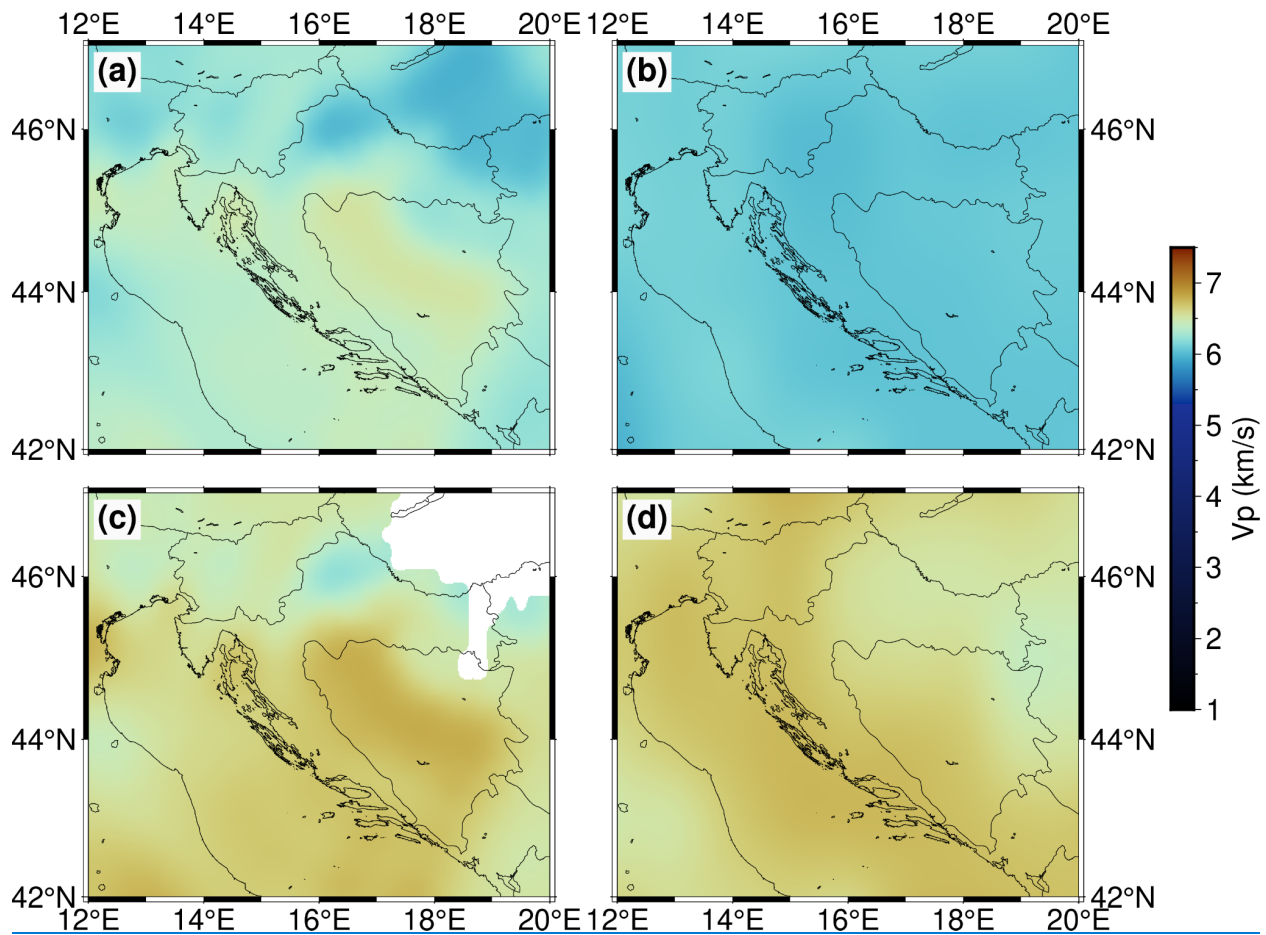


**Fig. D3** Comparison of P-wave velocity: (a) our model at 15 km depth, (b) EPcrust upper crust, (c) our model at 25 km depth, (d) EPcrust lower crust.

1295 [There is noticeable horizontal variation of velocity values in our model compared to the](#)  
[velocities defined in the EPcrust model, due to inclusion of data from refraction and](#)  
[gravimetric profiles.](#)